Chapter 1

INTRODUCTION

1 Defining Circulation

This course focuses on a particular subclass of ocean currents, $\mathbf{u}$, that we designate as the *circulation*. Circulation is characterized primarily by its persistence, and thus it is at the low-frequency end of the oceanic spectrum of variability. Persistent currents typically have a somewhat large spatial extent, on the order of tens of kilometers horizontally (comparable to the *deformation radius*, $R = NH/f$, where N is the Brunt-Väisälä or buoyancy frequency, H is the vertical scale of the current, and f is the rotation or Coriolis frequency; see Secs. 6-7 for more complete definitions) or larger. Other types of currents are tides, mesoscale eddies, waves (*i.e.,* acoustic, surface and internal gravity, inertial, coastal, equatorial, and Rossby), and turbulence, which are not the primary focus of this course. We shall also view storm-driven currents as too transient to include in the circulation category, but the response to time-varying climatic forcing, essentially starting with the seasonal cycle, is counted as circulation. Nevertheless, there are many ways transient, small-scale currents do matter to the dynamics of the circulation and thus must be included in our discussion. The most common form of their influence is as mixing or diffusion of large-scale quantities, but we more generally refer to their effects as *rectification*.

Most persistent currents occur in response to imposed forcings which themselves are persistent. The most important forcings are surface *wind stress* (a momentum source) and surface *heat and freshwater fluxes* (density or buoyancy sources) through exchanges with the atmosphere, sea ice, and rivers. The sea floor is usually only a weak source of heat or other materials—except locally at geothermal vents, mostly located along topographic ridges at sea-floor spreading sites—so it is usually assumed to be insulating and stationary, although exceptional circumstances do occur (*e.g.,* vents, tsunamis generated by earthquakes). The most persistent parts of air-sea flux are on a large spatial scale of many 100s or 1000s of km. So, much of the circulation is also large-scale, and this is referred to as the *general circulation*. It is a peculiarity of ocean dynamics, unlike atmospheric dynamics, that an essential part of the general circulation is also small-scale while still being persistent, *viz.,* the boundary and Equatorial currents which have tangential widths of $\mathcal{O}(10-100)$ km but such large velocities that their mass transports are comparable to (and often closing the mass balance with) the larger-scale interior currents. These important narrow currents have longitudinal scales as large as the scales of atmospheric forcing or oceanic basins. There are also persistent forcings that are smaller in scale. An example is a near-shore estuarine circulation, driven by a river outflow of freshwater into the salty ocean with consequent buoyancy and pressure-gradient forces that accelerate the circulation nearby.

In the same way that rectification effects of transient currents must be considered as relevant to circulation, so too are the scalar fields of temperature, T, and salinity, S that are relevant because

of their influence on the buoyancy field, hence on the gravitational force. There are no important internal sources of heat or salt in the ocean since phase changes occur only at the sides or near the surface, and the influx of dissolved salts from rivers and the bottom sediments is negligible on oceanic dynamical time scales of $\mathcal{O}(1000)$ yr or shorter. Thus, potential temperature, θ (*i.e., T* modified by adiabatic compression or expansion as the pressure of a parcel changes), and S are conservative *tracers* that move with the currents within the ocean, except for mixing by molecular diffusion. Other scalar fields have the same evolution dynamics (apart from their chemical and biological transformations), so they too are often considered along with the rest of the general circulation. Mass, of course, is the quintessential tracer because it evolves without any net effect from molecular diffusion in the nearly incompressible ocean.

Our knowledge of oceanic circulation comes fundamentally from measurements. Tracer measurements in the ocean have always been more abundant than velocity measurements (Sec. 5). Because of the approximate validity for the circulation of *hydrostatic* and *geostrophic* momentum balances (relating the buoyancy and velocity fields; Sec. 6), T and S measurements are often indicative of $\mathbf{u}$ structures. However, since the combination of geostrophy and hydrostacy is the so-called thermal-wind relation — but really the pycnal-wind, where "pycnal" refers to density — the T and S distributions determine only the vertical shear of the horizontal velocity, $\partial_z \mathbf{u}_h$. This leaves an undetermined *reference-level velocity* as a constant of vertical integration. There is a historical tradition of resolving this dilemma by assuming zero abyssal velocity (*i.e.,* a *level of no motion*), but this is not accurate for many purposes. At a more fundamental level, though, the quantitative inference of $\mathbf{u}$ from tracer distributions is an exceedingly difficult mathematical estimation problem; the so-called *inverse problem* for advection-diffusion dynamics has polluted the practice of observational oceanography because too many people have believed they could intuit the solution.

2 Motivations

What are some of the motivations for investigating oceanic circulation?

(a) *a description of reality*: what are the persistent currents in Earth's ocean?

(b) *a problem in physics*: given the tidal, wind, and buoyancy forcings, the material composition of seawater, and the shape of the basins, what are the resulting motions, the currents?

(c) *a problem in geophysical fluid dynamics*: what are the dynamical processes of oceanic circulation — characteristically involving density stratification (gravitationally stable almost everywhere), Earth's rotation, large Reynolds number (*i.e., $Re = VL/\nu$*, where V and L are velocity and length scales, and ν is the molecular viscosity), and two material influences on buoyancy, θ and S — that are also relevant to processes in engineering fluid behaviors, planetary atmospheres, stellar interiors, and space plasmas and gases?

(d) *a simulation challenge*: how can oceanic simulation models be formulated to help describe reality or solve the physics problem, either through comparison between model solutions and observational analyses or through assimilation of observations into model solutions?

(e) *Earth's climate*: how does the oceanic circulation combine with the other major internal components of the climate system — the atmosphere, land surface, ice, and biogeochemistry — to produce the mean and slowly varying states of the atmosphere under variable external influences, including anthropogenically induced changes (*e.g.,* global warming)?

(f) *Earth's history*: how has the ocean evolved, and what role has its circulation had in paleoclimates and the evolution of life?

(g) *environmental management*: how does oceanic circulation respond to and affect the consequences of human modifications of Earth, *viz.,* climate (*e.g.,* global warming), shoreline evolution (*e.g.,* erosion and flooding), pollution dispersal (*e.g.,* garbage, sewage, and toxic and radioactive materials), and the biosphere (*e.g.,* carbon cycling, fisheries, species diversity)?

(h) *military and commercial operations*: what dangers and opportunities does oceanic circulation provide for shipping, drilling, mining, fishing, mariculture, garbage disposal, and acoustic or cable signal transmission?

Please notice that most of these motivations are broader than just the scientific subject of physical oceanography. This is especially germane at UCLA since there is not yet a complete graduate curriculum in physical oceanography, and most students do not have this as their primary interest.

3   Types of Circulation

In order to provide a broad orientation in the phenomenology, what follows is a categorization of the principal types of circulation and brief descriptions of their causes and properties. In future lectures each type will be examined in more detail.

Planetary Boundary Layers (PBL)   (Chap. 2): These currents are located near the top and bottom boundaries within layers usually of 10-100 m depth, although the surface PBL depth can exceed 1000 m during *deep convection* (Figs. 1 and 11). They have an ageostrophic dynamics closely connected to the turbulent eddy fluxes generated by instability of the shear or buoyancy profile induced by the boundary fluxes; small-scale turbulence is particularly intense in the PBLs. However, they can also be superimposed on geostrophic currents near the surface of the many different types described below. The principal types of PBL currents are (1) wind-driven currents at the surface, as in the *Ekman velocity* but also often with buoyancy forcing influencing the vertical profile and with important influences from *Stokes drift* (*i.e.,* the average Lagrangian current associated with surface gravity waves) as well; (2) Ekman-like currents due to the drag of interior

geostrophic currents against the solid bottom; and (3) *gravity currents* flowing downslope by gravitational acceleration, entraining ambient fluid, and eventually being arrested through geostrophic adjustment (this is not very common because a sustained source of negative buoyancy at the bottom boundary is rare).

Extra-tropical Wind Gyres and Western Boundary Currents (WBC) (Chap. 3): Horizontal gradients in the wind stress, providing *wind curl*, act through *Ekman pumping* to create *Sverdrup transport* (Sec. 7) in extratropical basins with continental zonal (*i.e.,* east-west) boundaries. These are geostrophic currents mostly in and above the pycnocline (*i.e.,* within the top 1 km or less; see Fig. 1 for a typical buoyancy profile, Figs. 8-9 for meridional (*i.e.,* north-south) sections of mean T and S, and Fig. 11 for a cartoon of the meridional section density structure on various scales of motion). Due to the prevailing surface wind patterns of tropical and polar easterlies and mid-latitude westerlies, the characteristic gyre patterns are of two types:

- *Subtropical* (between the tropics and mid-latitudes) with anti-cyclonic flow ($\zeta/f < 0$, where $\zeta = \hat{\mathbf{z}} \cdot \mathbf{\nabla}_h \times \mathbf{u}$ is the vertical component of vorticity), hence a poleward western boundary current;

- *Subpolar* (between the mid-latitudes and polar regions) with cyclonic flow ($\zeta/f > 0$), hence an equatorward western boundary current.

The WBC exist essentially to return the oppositely flowing interior Sverdrup transport, but they also separate from the boundary near the climatological position of zero wind curl and extend eastward into the interior. These regions of strong current are always unstable to meanders and mesoscale eddies. Typical gyre transport strengths are several 10s Sv (1 Sv = 10^6 m^3 s^{-1}) due to the Sverdrup balance, with substantial eddy-driven enhancements in *recirculation zones* near the separation sites. Particular examples of these boundary currents are the Gulf Stream and Labrador Current in the North Atlantic, the Kuroshio and Oyashio in the North Pacific, the Brazil and Malvinas/Faulkland Currents in the South Atlantic, the East Australia Current in the South Pacific, and the Agulhas Current in the South Indian (Figs. 2, 3, 4, and 12).

Antarctic Circumpolar Current (ACC) (Chap. 4): Where there are no continental boundaries along lines of latitude, as between about 55-65° S, then a basin-scale, zonal pressure-gradient force cannot be supported to balance the meridional geostrophic Sverdrup transport (*i.e.,* as in $fv = \partial_x \phi$). In this latitude band a geostrophic eastward current > 100 Sv is directly driven by the westerly winds (Figs. 2, 4, 12). It reaches to the bottom with only a moderate decrease in its strength (unlike the more surface-intensified wind gyres). Equilibrium with the eastward surface stress occurs through the downward flux of momentum through the interior by mesoscale eddy fluxes (*i.e.,* by *isopycnal form stress*) and a westward bottom *topographic form stress* against the bottom.

The mean overturning circulation in the meridional plane (y, z) is ageostrophic in the ACC, again because there can be no mean zonal pressure gradient. It is often called the Deacon Cell and is dynamically analogous to the Ferrel Cell of the atmospheric Jet Stream. Its surface branch is equatorward Ekman transport; poleward return flow occurs at dept;, and the total transport is many 10s Sv (Fig. 5). However, this circulation is partly illusory with respect to material transport since there is a substantial cancellation by a mesoscale *eddy-induced Lagrangian mean circulation*, somewhat analogous to the Stokes drift of surface gravity waves. The ACC is also influenced by the deep branches of the thermohaline circulation (below), but how this occurs is a current research issue.

Arctic Gyre (Chap. 8): The Arctic Ocean also lacks continental boundaries along latitude lines and therefore has circulations directly driven by the wind stress, whose patterns are both zonal and gyral. Because the prevailing winds are not especially strong near the North Pole and because the usual ice cover sometimes acts to prevent stress transmission to the ocean, these gyres are fairly weak. The Arctic is one of many *marginal seas* that are in semi-enclosed basins with narrow passageways and that have modest mass exchanges with the broader basins and general circulation. The Mediterranean Ocean and Black Sea are other examples of a marginal sea.

Equatorial Currents (Chap. 5): Because $f = 0$ at the equator, Ekman and Sverdrup transport and geostrophic relations are less universally reliable. Nevertheless, meridional Ekman divergence away from the equator causes equatorial upwelling within the pycnocline, leading to somewhat colder surface temperatures on the Equator than off it. The surface easterly trade winds drive a near-surface, westward Equatorial Current (EC) (Figs. 2, 6, and 12) and an associated zonal pressure-gradient force due to high sea level, η ($\Rightarrow$ high subsurface pressure, $\phi = p/\rho_o$ with ρ_o the mean ocean density, by the hydrostatic relation), in the west. Beneath the PBL, this pressure-gradient force accelerates the eastward Equatorial Undercurrent (EUC) (Fig. 6) that also causes upwelling near the eastern boundary, hence a shallower pycnocline and colder surface temperatures there. There are also some Equatorial Counter Currents (ECC) away from the Equator (*e.g.,* the NECC near 10° N in Fig. 6a). These are a form of Sverdrup circulation in addition to the more extensive subtropical and subpolar gyres.

Thermohaline Circulation (THC) (Chap. 6): Planetary-scale buoyancy forcing is delicately balanced in its meridional contrasts: tropical heating and evaporation vs. polar cooling, precipitation, river outflow, and sea ice freezing and melting (which is most important due to brine rejection or dilution, respectively, since sea ice has a much lower S than seawater). Nevertheless meridional buoyancy gradients exist, hence hydrostatic pressure gradients exist, and a THC is accelerated. There is quite deep convection (*i.e.,* a deep PBL) in the sinking regions of the THC, and this induces very weak stratification in both T and S (see Figs. 8-9 near the Icelandic ridge around 65° N). In the present climate, these regions of *deep-water formation* are quite few and narrow.

The most important sinking region is in the North Atlantic (*i.e.,* Greenland and Labrador Seas), with a resulting *meridional overturning circulation* (MOC) mass flux of ~ 25 Sv (Figs. 5 and 7). The next most important sinking occurs in shallow water on the continental shelves near Antarctica (*i.e.,* Weddell and Ross Seas), with a strength < 10 Sv. Its connecting MOC can be seen in Fig. 5 as the counter-clockwise cells against Antarctica and near the bottom; although it appears to be interrupted by the clockwise Deacon Cell, this impression is misleading because of the eddy-induced cancellation of the latter (Chap. 4). There is also intermediate-depth convection in the Mediterranean Sea that causes an outflow of relatively dense, salty water into the Atlantic through the Strait of Gibralter; the effects of the latter can be seen in the mid-level S maximum near 35° N in Fig. 9. More local forms of THC also arise through buoyancy forcing on continental shelves and in estuaries.

The deep branches of the global-scale THC leave the sinking regions well below the pycnocline, primarily as Deep Western Boundary Currents (DWBC) but also as currents confined to the flanks of mid-ocean ridges and through deep topographic trenches (and perhaps as stacked equatorial zonal jets, but this is a current research topic.) The rising branches and near-surface, horizontal return flows towards the sinking regions are less geographically confined toward the western boundary.

Coastal Currents   (Chap. 8): In addition to the WBC and THC circulations near the boundaries, there are also along-shore coastal currents locally driven by along-shore winds. At an eastern boundary of a basin, such as the U.S. West Coast, an equatorward wind induces causes an off-shore surface Ekman flow and its off-shore horizontal divergence causes a compensating *upwelling* of cold and nutritious water near the boundary and a deep on-shore flow beneath the pycnocline (see Fig. 10). This in turn implies a cross-shore buoyancy gradient that is geostrophically balanced by an equatorward surface flow and a poleward undercurrent. The cross-shore scale of these coastal currents is on the order of the baroclinic deformation radius, $R \sim 10$s km. In addition to upwelling currents there are many other types of coastal currents: downwelling driven by convergent Ekman currents at the boundary, *estuarine* currents driven by surface and fluvial buoyancy fluxes, tidal and surface-wave rectified flows, island and headland wakes, along-shore currents driven by along-shore pressure gradients, *etc.*

Eastern Boundary Currents (EBC)   (Chap. 8): Fig. 2 shows relatively strong equatorward flow in the eastern parts of at least some of the major sub-tropical gyres: the California Current in the North Pacific, the Humbolt Current in the South Pacific, and the Benguela Current in the South Atlantic for sure, and perhaps the Canary Current in the North Atlantic and the West Australia Current in the South Indian. Their off-shore scales are many 100s of km, wider than the WBC of the wind gyres or the upwelling coastal currents, each of $\mathcal{O}(R)$. There is not yet a clear understanding of whether these are simply a manifestation of Sverdrup transport, if indeed there is anomalously large wind curl near eastern boundaries (perhaps because of a large-scale, sea-breeze enhancement of the mid-latitude westerlies that is not yet empirically well determined), or a long-time

equilibrium state of seasonally and synoptically forced coastal currents.

Passage Currents   (Chap. 8): Topography influences circulation in many different ways, *e.g.,* steering currents approximately along isobaths and providing form stress (as in the ACC). Topography is particularly important when large-scale forcing drives currents through narrow passages, where the boundary-area to interior-volume ratio is unusually large. There the bottom PBLs can occupy a substantial fraction of the volume, so small-scale turbulence can be quite influential in providing anomalous damping, drag, mixing, and dissipation. In some instances the circulations reach a state of *hydraulic control* (this also occurs in flow over a weir), where the relevant Froude number stays near its critical value of one, $Fr = V/NH = 1$. Examples of flows thought by some to be in a state of control are in the Indonesian Throughflow, the Strait of Gibralter, and deep branches of the THC along the axes of bottom trenches (*e.g.,* , the northward flow of Antarctic Bottom Water (AABW), through the Vema Gap into the North Atlantic; Fig. 13). In each of these cases the proximate cause of the circulation is a large-scale pressure-gradient force.

4   Measurement, Theory, and Modeling in Oceanography

The science of oceanic circulation is difficult and messy, in ways that are also shared with atmospheric science and astronomy, each in somewhat different ways. Therefore, we should be sensibly humble in our expectations: the understanding we are likely to achieve usually will be fragmentary and partial rather than comprehensive, and the rate of progress is more likely to gradual rather than having many dramatic discoveries.

Scientific knowledge is fundamentally based on measurements, and the social culture of oceanography has always given its greatest respect to those who make them. Sec. 5 lists the common methods of making ocean measurements, both historical and modern. However, the sampling limitations — *i.e.,* the limited number and space/time distribution of measurements — are extraordinarily difficult to overcome in oceanography, given the broad-band wavenumber and frequency spectra for oceanic fields. It is hard to imagine ever having enough measurements to adequately describe the circulation; in this regard, oceanic data is far sparser than atmospheric data. It is laborious and expensive to place and recover instruments deep within the ocean well away from land. Traditionally this is done by lowering instruments from ships (usually to sample T, S, p and other chemical concentrations) or from mooring them on tethers attached to bottom weights (usually current meters), with ships required to deploy and recover the moorings. Instrument motion, because of ship or mooring motion, often contaminates current measurements.

There are trends in instrumentation that are improving this sad situation, though they are not likely to wholly reverse it. Autonomous, freely drifting or self-navigating platforms are far cheaper than conventional shipboard or moored platforms. Acoustic tracking or satellite navigation to determine the positions of floats and drifters, as well as telemetry of other *in situ* measurements

helps both with timeliness and expense (Fig. 14 has a composite of interior float trajectories in the North Atlantic). A global and sustained deployment of profiling floats (called ARGO) is now being started by many nations. Remote sensing is also useful. Acoustic sampling is a potentially powerful methodology — either through sound scattering off of suspended particles or density gradients (sonar) or through statistical inversion of sound transmission times for the velocity and thermodynamic fields through which the propagation occurs (tomography) — although the signals from such measurements are still quite challenging to interpret. Remote sensing of the sea surface can occur with electromagnetic sampling by radiometers (passive) or radars (active), either from airplanes (which are expensive to fly) or from satellites (which are even more expensive but have richer sponsors to support them). Land-based radars use Doppler backscatter to infer the surface current; at present they are useful only for short distances from land, ~ 10 km, but this range is now being expanded by an order of magnitude. Satellite instruments can measure surface wave properties by radar, which also contain information about currents and chemical composition (primarily surfactants through their dynamical influence on the waves); sea-surface T and certain aspects of chemical composition (i.e., "color") by radiometry; and η by altimetry, which is the surface geopotential (or dynamic height) field once the local gravitation reference potential is subtracted (which is challenging since gravitational equipotential surface elevations vary by ~ 10 m, whereas the oceanic dynamic signal is typically ~ 0.1 m). Since seawater is nearly impenetrable to electromagnetic radiation, such sampling is confined to near the surface. One of the most important scientific questions in oceanography is how well surface measurements can be used to diagnose interior quantities, via data assimilation or other statistical estimation methods.

Satellite altimetry (Chelton et al., 2001) is perhaps the most important of these advances, because of its unparalleled sampling density (global coverage with ~ 100 km spacing between ground tracks every ~ 10 days), precision ($\sim$ cms in η with the current instruments), and rather direct relation to surface currents through the geostrophic balance,

$$\mathbf{u}(0) \; \approx \; -\frac{g}{f}\,\hat{\mathbf{z}} \times \boldsymbol{\nabla}\eta,$$

once corrections have been made for the tides (which are aliased because of the pattern of satellite orbits), atmospheric water vapor (which refracts the radar pulses); atmospheric surface pressure fluctuations (which usually induce an *inverse barometer* response,

$$\eta \; \approx \; -\frac{1}{g}\,\phi_{atm}\,,$$

such that η adjusts to leave the hydrostatic, sub-surface ϕ unvarying; an electromagnetic scattering bias for the radar reflection off the rough sea surface; and a wave-averaged mean surface-gravity-wave contribution (Chap. 2). It is quite a complicated and technically difficult measurement methodology (Fig. 15). Its greatest limitation for estimating the time-mean circulation is the presently poor knowledge of Earth's gravitational field, the *geoid* or surfaces of constant gravitational potential. The errors increase as on smaller scales (Fig. 16): the signal/noise cross-over scale is at a wavelength of about 4000 km (*i.e.,* spherical harmonic of degree $n \approx 10$). Thus, the time-mean η is only known from altimetry on very large scales, comparable to the gyre patterns in

8

the interior, but not to the equatorial or western boundary currents (Figs. 17-18). A current satellite mission (called GRACE) is reducing the cross-over scale by about an order of magnitude and thus will greatly improve the utility of the mean field estimates; a preliminary product from GRACE is shown in Fig. 19. The geoid estimation problem, of course, does not apply to time variability of η, since the geoid error is steady in time. Thus, altimetric maps of $\overline{\eta'^2}(x, y)$ (excluding the contributions from surface gravity waves and tides) provide the best available empirical information about circulation variability.

Laboratory experiments have a very limited potential to be generally useful in the science of oceanic circulation because viscosity exerts too much control on the dynamics, given the small size of laboratory tanks and the appreciable molecular diffusivities of ordinary fluids. Of course, there are some particular issues where laboratory measurements have been valuable, such as investigating *double diffusion* — currents influenced by the different molecular diffusivities of T and S — which is a phenomenon with an inherently small Reynolds number.

Theory and modeling of oceanic circulation are limited by the intrinsic difficulty of solving the governing equations; by the very large number of degrees of freedom with significant variance; and by the geographic complexity of both the forcing and the domain shape. Of course, incomplete empirical knowledge of the forcing fields by itself precludes an accurate solution of a purely oceanic problem. In this regard, we can hope to obtain more fundamental and reliable solutions for the climate problem as a whole, given the relatively well measured solar radiation field as its forcing, but this is an even much larger and more difficult problem in physics in many other aspects.

The comparative strengths of analytic theory and numerical computation for oceanic circulation are the usual ones: greater rigor and comprehensibility for the former and greater capability for solving harder problems for the latter. Given the great difficulties of oceanic problems and the continuing, rapid technological progress in computing capabilities, — and potentially algorithmic progress as well, although oceanographers, as the meteorologists, have been somewhat backward in this regard — we can confidently expect the relative importance of modeling to increase with time (barring the unlikely discovery of radically new and more powerful methods of mathematical analysis). It is perhaps a somewhat more uncertain forecast to say what the relative importance of measurement and modeling will be in the future, but an extrapolation of their previous rates of technological progress would favor modeling judged by the standard of the information density to be obtained. Of course, measurements will remain the prime arbiters of physical reality, and model solutions must always be checked with measurements as thoroughly as possible.

Numerical models can be devised for all scales of currents, from turbulence, ~ 1 m, to planetary circulation, $\sim 10^7$ m, and with varying degrees of mathematical idealization or simulated realism. Of course these different regimes cannot be encompassed within the same model because the size of the computation would be excessive. So different problems must be posed for different regimes, with the important effects of the unresolved dynamics imposed in some fashion, usually either as a forcing or a sub-grid-scale parameterization. Also, model problems can be posed with a wide range between idealization or complexity; reliability and interpretability are more likely to be achieved for idealized problems, but realism exerts a pull towards greater complexity.

Oceanic General Circulation Models (OGCMs) are devised with the goal of being as complete and realistic as is computationally feasible, starting both from the largest spatial scale of the domain (the globe or an oceanic basin) and reaching downwards as far as the size of the spatial grid allows, and from the shortest temporal scale required for computational stability of the integration (typically $\sim$ 10^3 s) and reaching upwards as far as the length of computation that can be afforded. Often one needs a domain as large as a basin for a dynamically well-posed boundary-value problem — containing, say, a complete wind-gyre recirculation pattern — in order to escape the computationally and physically difficult problem of adequately specifying open-water boundary conditions; however, there are some situations (*e.g.,* the California Current System; Marchesiello et al. (2001)) where outward propagation or radiation conditions suffice. There is a critical spatial grid resolution threshold for an OGCM, $\sim$ 10 km, associated with mesoscale eddies and inertial boundary currents, and OGCM usage is split into *eddy-resolving* and non-eddy-resolving calculations. (This dilemma is not significant for atmospheric GCMs since the energetic eddy scale, for synoptic storms, is much closer to the planetary scale of the domain.) There is also a critical temporal duration threshold, $\sim$ 10 yr, associated with going beyond the spin-up of basin-scale wind-driven currents by means of baroclinic Rossby wave transits of the basin, to the adjustment times for the material property distributions, $\sim 10^3$ yr, associated with small material fluxes across interior isopycnal surfaces (*i.e.,* diapycnal fluxes). This modeling dilemma also does not occur as acutely in the atmosphere, where dynamical adjustments are completed within $\sim$ 1 mo. and material property distributions equilibrate within $\sim$ 1 yr. There is a standard approach to the design of an OGCM, begun by Bryan (1969) more than 30 years ago and based upon the hydrostatic Primitive Equations (PE) and low-order finite differencing. Only recently have alternatives — such as solving the PE in either terrain-following (i.e., σ) or pseudo-isopycnal coordinates (because interior currents are very nearly adiabatic and isentropic) or use of the more general Boussinesq Equations — been given serious attention. But it is a lengthy and laborious path to develop and test a comprehensive OGCM, so it is presently unclear how advantageous such alternatives may become. To read more about OGCMs you can refer to my review articles (McWilliams, 1996, 1998) and Chap. 7.

In this course, I shall spend little time talking about ocean measurements, but I shall present various observational summaries to demonstrate relevant phenomena. I shall also spend more time on analytic theory than numerical solutions because this allows the conceptual framework of the oceanic circulation to be communicated more explicitly and concisely. However, for those of you who intend to do original research on oceanic circulation, I advise you that the power of computations probably makes this the most fruitful approach, although every scientist has to decide which methods they feel most comfortable working with.

5 Oceanic Measurement Types

Here I use an outline format rather than a full text. For further brevity, the following symbols are used to indicate how useful the different measurement types are:

$^{\#}$ with widespread modern utility

$^{?}$ with at least the potential for widespread utility.

The bracketed comments (with exclamation points) refer to important technical challenges.

sea level η:

- tide gauge (coast) [leveling!]

- altimeter$^{\#}$ (satellite) [gravity field! satellite tracking! surface-waves!]

pressure, ϕ:

- barometer [high abyssal pressure!]

- strain gauge (ship cast$^{\#}$, mooring/float$^{\#}$, bottom [instrumental motion and signal drift!])

temperature, T:

- thermometer (bucket)

- reversing thermometer (ship cast)

- intake thermograph (ship)

- bathythermograph (ship cast): MBT, XBT$^{\#}$

- thermister$^{\#}$ (drifter, float, mooring)

- CTD$^{\#}$ (ship cast)

- radiometer (plane, satellite$^{\#}$) [clouds! skin depth!]

- acoustic tomography$^{?}$, via travel time, $\int dx/C_{sound}(T, S, p)$ (mooring) [sound sources! data inversion!]

salinity, S:

- bottle sample & titration (ship cast)

- intake salinograph (ship)

- conductivity sensor (mooring, drifter, float) [sensor drift!]

- CTD[#] (ship cast)

- XCTD[?] (ship cast) [sensor drift!]

- satellite sensor[?]

velocity, $\mathbf{u}_h$:

- surface drifter: bottle (coast), drogued & radio-tracked (ship, plane, satellite[#]) [slippage! PBL profile inversion!]

- current meter[#], mechanical or acoustic (mooring) [mooring motion!]

- float[#]: acoustically tracked, *e.g.,* SOFAR or RAFOS [sound source!], or cycling to surface and radio tracked, *e.g.,* PALACE [bias introduced on vertical cycle!], usually iso-p but sometime iso-ρ.

- acoustic Doppler profiler[#], *e.g.,* ADCP (ship or mooring)

- surface backscatter radar[?], *e.g.,* CODAR (coastal) [range! wave bias!]

- electric field, via $\mathbf{E} = \mathbf{u} \times \mathbf{B}_{earth}/C_{light}$ (ship cast, bottom cable) [calibration! deployment!]

. . . plus various instruments for chemical concentrations and air-sea fluxes.

6 Fundamental Ocean Dynamics

The essential fluid dynamics of currents in the ocean are expressed, with generally sufficient accuracy, in the rotating Boussinesq equations with an empirically determined equation of state, $\mathcal{R}$:

$$
\begin{aligned}
\frac{D\mathbf{u}}{Dt} + 2\mathbf{\Omega} \times \mathbf{u} &= -\mathbf{\nabla}\phi - \frac{g}{\rho_o}(\rho - \rho_o)\hat{\mathbf{z}} + \nu\nabla^2\mathbf{u} \\
\mathbf{\nabla} \cdot \mathbf{u} &= 0 \\
\frac{D\theta}{Dt} &= \kappa_\theta\nabla^2\theta \\
\frac{DS}{Dt} &= \kappa_S\nabla^2 S \\
\rho &= \mathcal{R}[\theta, S, z],
\end{aligned}
\tag{1}
$$

where $\mathbf{u}$ is the velocity, $\mathbf{\Omega}$ is Earth's angular rotation (*n.b.,* its magnitude is 1.4×10^{-4} s^{-1} and its orientation is upwards from the North Pole), $\phi = p/\rho_o$ is the geopotential (with p the dynamic pressure), g is gravitational acceleration, ρ is density (with ρ_o its mean value), $\hat{\mathbf{z}}$ is the upward unit vector (opposite to gravity), ν is molecular viscosity, θ is the potential temperature, κ_θ is molecular thermal diffusivity, S is the salinity, κ_S is molecular haline diffusivity, and

$$
\frac{D\cdot}{Dt} = \frac{\partial\cdot}{\partial t} + \mathbf{u} \cdot \mathbf{\nabla}\cdot
$$

is the advective time derivative.

7 Approximate Circulation Dynamics

Later in the course we shall pose and solve many different boundary-value problems for different circulation regimes. In the meantime we review here some dynamical approximations and diagnostic relations, commonly used as aids in interpreting measured phenomena. However, they should not be presumed to be reliable without checking in any particular situation. Our focus is on large-scale, low-frequency circulation. We assume that Earth's rotation and stable stratification are important in the force balance, but time dependence (*i.e.,* acceleration) is often secondary. In many of the relations below, time dependence is entirely absent (*i.e.,* they are *diagnostic* rather than *prognostic*).

7.1 Primitive Equations in a Thin Spherical Shell

The hydrostatic approximation to the vertical momentum balance in (1) is

$$
\frac{\partial\phi}{\partial z} \approx -\frac{g}{\rho_o}(\rho - \rho_o) \equiv b,
\tag{2}
$$

where b is buoyancy. The Primitive Equations (PE) make this approximation, usually along with approximating the rotation vector in the Coriolis force by its local vertical component,

$$2\mathbf{\Omega} \;\approx\; f\hat{\mathbf{z}}, \quad f(\varphi) \;=\; 2|\mathbf{\Omega}|\sin[\varphi], \tag{3}$$

where φ is latitude. Both approximations are justifiable by a thinness assumption, $H/L \ll 1$, appropriate to large-scale currents in the ocean. When expressed in spherical coordinates, (λ, φ, z) — *n.b.*, there are subtleties associated with the diffusion terms in these coordinates; see Bryan (1969) — the PE comprise the dynamical basis for almost all OGCMs (Chap. 7).

7.2   Equation of State and Stratification

The equation of state for seawater is known only as a fit to measurements (Jackett and McDougall, 1995) since it has no theoretical derivation from molecular dynamics (unlike a dilute gas). It is usually expressed in terms of the state variables (T, S, P), where P is the total pressure. There are complicated computational formulae for *in situ* density $\rho(T, S, p)$ and for potential temperature $\theta(T, S, P; P_{ref})$, where P_{ref} is the reference pressure for the implied adiabatic comparison, as well as other thermodynamic properties such as heat capacity or sound speed. Adiabatic motions preserve potential density $\rho_\theta(T, S, P; p_{ref})$, which can also be expressed as $\rho_\theta(\theta, S; P_{ref})$. The buoyancy frequency N is related to ρ_θ by

$$N^2 \;=\; -\frac{g}{\rho_o}\frac{\partial \rho_\theta}{\partial z}, \tag{4}$$

and it is the fundamental oscillation frequency for a parcel adiabatically displaced in a stably stratified environment in the neighborhood of $P = P_{ref}$. For the state variables in $\mathcal{R}$ in (1), T is replaced by θ, because of the latter's simple isentropic conservation law, and P is replaced by z, because the hydrostatic estimate using mean density, $P \approx -g\rho_o z$, is sufficiently accurate.

The nonlinearities in $\mathcal{R}$ give rise to peculiar behavior under some circumstances. One is that the mixing of two parcels with initially the same value of ρ_{pot} but different values of (θ, S) can yield the averaged values for (θ, S) but a different value for ρ_{pot}, thus giving rise to an unbalanced buoyancy force, hence an acceleration of the mixed parcel; two specific ways this occurs are called *caballing* and *thermobaricity*. Another peculiarity is that ρ_{pot} is not globally reliable as an indicator of gravitation stability if parcels move far from $P = P_{ref}$; *e.g.,* a pair of parcels stably aligned with lighter ρ_{pot} above heavier in the abyss may become unstably aligned if brought adiabatically to the surface, which also would induce an acceleration. Thus, where these peculiarities might matter, it is desirable to use a local P_{ref} to determine the stratification. One such procedure is to define a global *neutral surface* as one on which small adiabatic displacements of any fluid parcel do not produce any buoyancy restoring forces on the parcel (McDougall, 1987). A neutral surface is everywhere tangent to an isopycnal (*i.e.,* with constant ρ_{pot}) surface based on the *in situ* value for P_{ref}; however, over large distances a neutral surface can depart substantially from any potential density surface with a fixed value of P_{ref}. In practice, the distinction between neutral and isopycnal

surfaces only becomes consequential when $P - P_{ref}$ is $\mathcal{O}(10^3)$ db (equivalent to a Δz of $\mathcal{O}(10^3)$ m).

Since large, rapid vertical parcel displacements are rare in the generally stably stratified ocean, some simplifying approximations are

$$\rho_\theta \approx \rho, \quad \theta \approx T, \tag{5}$$

and these are valid as long as parcels do not greatly change their pressure or depth on the time scale of dynamical interest (*i.e.,* ΔP is not too large), and

$$\rho \approx \rho_o \left(1 - \tilde{\alpha}(T - T_o) + \tilde{\beta}(S - S_o) \right), \quad \tilde{\alpha}, \tilde{\beta} > 0, \tag{6}$$

which is valid for small ΔP, ΔT, and ΔS. $\rho_o \approx 1.25 \times 10^3$ kg m^{-3} is a mean density of seawater, T_o and S_o are local reference values, and $\tilde{\alpha} \leq 2 \times 10^{-4}$ K^{-1} and $\tilde{\beta} \approx 8 \times 10^{-4}$ o/oo^{-1} are the thermal-expansion and haline-contraction coefficients, respectively.

7.3 Coriolis Force

With the approximation stated above for the PE, the Coriolis force is

$$2\mathbf{\Omega} \times \mathbf{u} \approx f(\varphi)\hat{\mathbf{z}} \times \mathbf{u}_h, \tag{7}$$

where $\mathbf{u}_h$ is the horizontal velocity. Common further approximations of f are

$$f \approx f_o \tag{8}$$

(f-plane), with $f_o = 2|\mathbf{\Omega}| \sin[\varphi_o]$, and

$$f \approx f_o + \beta(y - y_o) \tag{9}$$

(β-plane), with $\beta = \frac{2|\mathbf{\Omega}|}{a} \cos[\varphi_o]$. $\mathbf{\Omega}$ is the rotation vector for Earth, $a \approx 6.35 \times 10^6$ m is the radius of Earth, and $y = a\varphi$ is a local Cartesian meridional coordinate ($x = a\cos[\varphi_o]\lambda$ is its zonal counterpart). Note that f and f_o change sign across the equator, whereas β is always positive.

7.4 Geostrophic Balance

When the Rossby number, $Ro = V/fL$ is moderately small, the horizontal momentum equation in (1) or the PE simplifies to

$$f\hat{\mathbf{z}} \times \mathbf{u} \approx -\mathbf{\nabla}\phi, \tag{10}$$

which can be rewritten for the velocity as

$$\mathbf{u}_h \approx \frac{1}{f}\hat{\mathbf{z}} \times \mathbf{\nabla}\phi, \tag{11}$$

15

or for the vertical shear as

$$\frac{\partial \mathbf{u}_h}{\partial z} \approx \frac{1}{f}\hat{\mathbf{z}} \times \boldsymbol{\nabla} b \,. \tag{12}$$

The last relation is often called the *thermal wind* when $b \approx \alpha g T$. See Fig. 20 for some illustrations of (10)-(12). These relations are widely used for relating tracer observations and velocity, but they must be used with particular care in the tropics or near the boundaries.

7.5 Ekman Transport, Bottom Drag, and Ekman Pumping

In a steady, horizontally uniform boundary layer for a uniform-density, rotating fluid with an imposed surface (wind) stress, $\boldsymbol{\tau}^t$, at the top, the vertically integrated horizontal volume transport is

$$\tilde{\mathbf{T}}_{ek}^t \approx -\frac{1}{\rho_o f}\hat{\mathbf{z}} \times \boldsymbol{\tau}^t \,, \tag{13}$$

where

$$\tilde{\mathbf{T}}_{ek}^t \equiv \int_{-\infty}^0 \mathbf{u}_h^t \, dz \,. \tag{14}$$

In practice the lower limit of integration is taken as $h_{ek} \sim \sqrt{|\tau|/\rho_o}\,/\,f \sim 100$ m, or even less if there is a stable pycnocline nearer the surface to compress the boundary layer. Thus, the Ekman transport is directed 90° to the right [left] of the wind in the Northern [Southern] Hemisphere. This relation is used for determining the surface boundary-layer transport from the surface wind stress. (This transport is incremental to whatever horizontal transport is associated with geostrophic currents.) This formula must be used with care in the tropics, since (13) becomes singular at $f = 0$, and it is significantly modified by surface gravity waves under some conditions (Chap. 2).

A similar relation can be derived for the boundary-layer transport due to the drag of the current just above the bottom PBL, $\mathbf{u}_h(-H^+)$, as a consequence of $\mathbf{u} = 0$ (no slip) at the solid bottom, $z = -H$:

$$\tilde{\mathbf{T}}_{ek}^b \approx \frac{1}{\rho_o f}\hat{\mathbf{z}} \times \boldsymbol{\tau}^b = -\sqrt{\frac{\nu_v}{2|f|}}|\mathbf{u}_h(-H^+)|\,\hat{\mathbf{s}} \,, \tag{15}$$

where $\boldsymbol{\tau}^b$ is the bottom stress and ν_v is the eddy viscosity associated with the vertical momentum flux by the boundary-layer turbulence and $\mathbf{s}$ is a unit horizontal vector 135° to the left [right] of $\mathbf{u}_h(-H^+)$, in the Northern [Southern] Hemisphere. The final right-hand side assumes that ν_v is a constant, which is not a particularly accurate assumption within planetary boundary layers (*i.e.,* $\nu_v(z)$ has a parabolic profile, vanishing at the top and bottom of the layer; Large et al. (1994)). Sometimes an alternative quadratic bottom-stress law is used — instead of the Ekman-layer relation in (15) — with $\boldsymbol{\tau}^b = \rho_o C_D|\mathbf{u}_h|\mathbf{u}_h(-H^+)$ where $C_D \sim 10^{-3}$ is the drag coefficient. Under most circumstances in the ocean, $|\tilde{\mathbf{T}}_{ek}^b| \ll |\tilde{\mathbf{T}}_{ek}^t|$, so that most of the balancing horizontal mass flux for the surface Ekman transport occurs within the ocean interior as geostrophic currents both away from the side boundaries and in the WBC; the latter are established through a vertical mass flux between the surface PBL and the interior, called *Ekman pumping*.

By using the continuity relation in (1) and interpreting the Ekman boundary-layer transport relations above to include large-scale gradients in $\boldsymbol{\tau}$ and $\mathbf{u}_h(-H)$ parametrically, we can vertically integrate across the relatively thin surface and bottom boundary layers to calculate the vertical velocity w at the interior edges of the PBLs:

$$
\begin{aligned}
w^t &= \hat{\mathbf{z}} \cdot \boldsymbol{\nabla} \times \left(\frac{1}{\rho_o f} \boldsymbol{\tau}^t \right) \\
w^b &= \sqrt{\frac{\nu_v}{2f}} \, \zeta(-H) \,,
\end{aligned}
\tag{16}
$$

where $\zeta(-H)$ is the vertical component of vorticity in the adjacent interior, $\hat{\mathbf{z}} \cdot \boldsymbol{\nabla} \times \mathbf{u}_h(-H)$. These relations assume that $w = 0$ at the (flat) top and bottom surfaces, $z = 0, -H$; while this is not is precisely true for the ocean, it is generally a good enough approximation for at least the top surface.[1] Whether or not w^b is comparable to w^t depends upon the magnitude and horizontal scale content for $\mathbf{u}_h(-H)$ and $\boldsymbol{\tau}$, but w^b is often negligible for basin-scale currents (*e.g.,* in wind gyres), in part because $\mathbf{u}_h$ usually is much weaker in the abyss than in the pycnocline. We shall see that Ekman pumping induces both geostrophic and ageostrophic interior circulations (*e.g.,* the shallow MOC cells in Fig. 5).

7.6 Planetary Vorticity Balance and Sverdrup Transport

The vertical vorticity equation for basin-scale currents in the interior (outside the PBLs) takes the simple form of the curl of the geostrophic balance relation,

$$
\hat{\mathbf{z}} \cdot \boldsymbol{\nabla} \times (f \hat{\mathbf{z}} \times \mathbf{u}_h + \boldsymbol{\nabla}\phi) = 0 \,,
$$

when the relative vorticity ζ and its tendency are weak enough, as they are when L and t are sufficiently large (*i.e.,* when Ro is very small). Further, using the continuity relation in (1) yields

$$
\beta v_g \approx f \frac{\partial w}{\partial z} \,,
\tag{17}
$$

where the subscript g refers to the geostrophic velocity defined in (10).

We next decompose the total horizontal mass transport, $\tilde{\mathbf{T}}$, into boundary layer contributions

---

[1]If the bottom elevation varies spatially (*i.e.,* $z = -H = -H_o + B(\mathbf{x}_h)$), then vanishing normal velocity at the bottom implies that $w(-H) = \mathbf{u}_h(-H) \cdot \boldsymbol{\nabla}_h B$. In this case the pumping velocity at the interior edge of the bottom PBL is the linear sum of the two effects,

$$
w^b = \sqrt{\frac{\nu_v}{2f}} \, \zeta(-H) + \mathbf{u}_h(-H) \cdot \boldsymbol{\nabla}_h B \,.
$$

and an interior geostrophic contribution,

$$
\begin{aligned}
\tilde{\mathbf{T}} &\equiv \int_{-H}^{0} \mathbf{u}_h \, dz \\
&= \tilde{\mathbf{T}}_{ek}^{t} + \tilde{\mathbf{T}}_{g} + \tilde{\mathbf{T}}_{ek}^{b} \, .
\end{aligned}
\tag{18}
$$

Combining the relations (13), (15), (16), and the vertical integral of (17), we obtain

$$
\tilde{T}^{(y)} \approx \beta^{-1} \left(\hat{\mathbf{z}} \cdot \boldsymbol{\nabla} \times \boldsymbol{\tau}^{t} - r\zeta(-H) \right) ,
\tag{19}
$$

where $r \equiv \sqrt{\frac{f\nu_v}{2}}$ is an Ekman damping rate due to the bottom Ekman drag. Usually the last term is ignored, in which case we obtain the *Sverdrup transport relation* for the meridional transport,

$$
\tilde{T}^{(y)} \approx \frac{1}{\rho_o \beta} \, \hat{\mathbf{z}} \cdot \boldsymbol{\nabla} \times \boldsymbol{\tau} .
\tag{20}
$$

The Sverdrup transport circulation is completed by using the vertical integral of the continuity relation in (1). This shows that

$$
\boldsymbol{\nabla}_h \cdot \tilde{\mathbf{T}} = 0
$$

using a surface kinematic boundary condition of $w = 0$ at $z = 0$ (*i.e.,* the *rigid-lid* approximation, suitable for most currents but not for surface gravity waves). Hence we can define a horizontal transport streamfunction, $\Psi(x, y)$ (*cf.,* Fig. 4), such that

$$
\tilde{\mathbf{T}} = \hat{\mathbf{z}} \times \boldsymbol{\nabla}_h \Psi \, .
\tag{21}
$$

Substituting this into (20) and integrating zonally (assuming no mass flux through the eastern boundary at $x = L_x$ and a wind curl independent of x), we obtain

$$
\Psi = \frac{1}{\rho_o \beta} \left(\hat{\mathbf{z}} \cdot \boldsymbol{\nabla} \times \boldsymbol{\tau} \right) \left(L_x - x \right) .
\tag{22}
$$

This latter assumption is based on the empirical knowledge that EBCs are weaker than WBCs and the theoretical result that this fact is a consequence of $\beta > 0$ (Chap. 3).

The Sverdrup relation diagnoses the depth-integrated horizontal (*i.e.,* barotropic) transport from the curl of the wind stress. In places where isopycnals (*i.e.,* surfaces of constant density) intersect sloping bottom topography, there can be an important correction to the Sverdrup balance due to a topographic form stress (sometimes called *JEBAR*, the Joint Effects of Baroclinicity and Relief). In places where L and/or t are not so large (*e.g.,* in strong, narrow currents or in propagating Rossby waves), then the planetary vorticity balance and Sverdrup transport relations are invalid.

7.7 Planetary Geostrophic Potential Vorticity

Neglecting molecular diffusion and compressibility effects, the Boussinesq Equations (1) conserve *Ertel potential vorticity*, Q_{ert}, following parcels along their trajectories. For basin-scale motions,

we can approximate Q_{ert} as

$$
\begin{aligned}
Q_{ert} &\equiv (f\hat{\mathbf{z}} + \boldsymbol{\nabla} \times \mathbf{u}) \cdot \boldsymbol{\nabla} b \\
&\approx Q_{pg} \equiv f b_z = f N^2 \,.
\end{aligned}
\tag{23}
$$

The corresponding potential vorticity equation is

$$
\frac{DQ_{pg}}{Dt} = N.C.T. \,,
\tag{24}
$$

where $N.C.T.$ generically denotes of non-conservative effects from both molecular diffusion and rectification of sub-basin-scale currents (*e.g.,* turbulent transport). (24) is called the *Planetary Geostrophic potential vorticity equation* (PG). The approximations that underlie and accompany PG are hydrostatic and geostrophic balances, incompressibility, and $\frac{Db}{Dt} \approx N.C.T.$. PG is an approximate evolutionary (*i.e.,* prognostic) equation for extra-tropical, basin-scale currents, frequently used to analyze long baroclinic Rossby waves (*i.e.,* with $L \gg R$) and wind-gyres away from the neighborhood of the WBC and its separated westerly extension into the basins.

7.8   Quasigeostrophic Potential Vorticity

The classical geophysical fluid dynamical approximation for $Ro \ll 1$ is not PG but *quasigeostrophy* (QG), which originated in atmospheric theory. If, instead of the preceding basin-scale assumptions, we assume that $Ro = V/fL$, $Fr = V/NH$, and $Ro_\beta = \beta L/f$ are all comparably small non-dimensional parameters (hence $L \sim R$), then an asymptotic expansion yields QG at leading order:

$$
\frac{Dq_{qg}}{Dt_g} \approx N.C.T. \,,
\tag{25}
$$

where

$$
\begin{aligned}
q_{qg} &= \beta y + \nabla_h^2 \psi + f_0^2 \Big[\frac{\psi_z}{N^2(z)}\Big]_z \\
\frac{D}{Dt_g} &= \frac{\partial}{\partial t} + (\mathbf{u}_g \cdot \boldsymbol{\nabla}_h) \\
\mathbf{u}_g &= \hat{\mathbf{z}} \times \boldsymbol{\nabla}_h \psi, \quad \psi = \frac{1}{f_o}\phi \,.
\end{aligned}
\tag{26}
$$

(In contrast, PG assumes $Ro \ll Fr \sim Ro_\beta$ (hence $L \gg R$) and allows the latter two parameters not to be especially small.) For oceanic theory, QG is an useful approximate prognostic equation for extra-tropical mesoscale eddies and inertial boundary currents (*e.g.,* WBCs), and even for at least the essential behavior of wind gyres and the ACC.

19

8 Eddy Diffusion

Although the primary focus of this course is on the mean circulation, we do need to consider how transient and often smaller-scale currents dynamically influence the circulation (*i.e.,* rectification). Perhaps the most common formal representation of rectification effects is as a Reynolds stress and other time-mean property fluxes by eddies. A fluctuating current $\mathbf{u}'$ can have mean correlations with itself such that it provides a force acting on the mean current $\overline{\mathbf{u}}$; assuming $\overline{\mathbf{u}'} = 0$, this can be expressed as

$$\frac{\partial \overline{\mathbf{u}}}{\partial t} \;=\; \ldots \;-\; \boldsymbol{\nabla} \cdot \left(\overline{\mathbf{u}'\mathbf{u}'} \right)\,, \tag{27}$$

where the dots indicate other deleted terms in the equation and $\overline{\mathbf{u}'\mathbf{u}'}$ is the Reynolds stress or eddy momentum flux. There are analogous relations for advected scalar quantities, c, such as potential temperature, salinity, potential vorticity, or any other *material property* (*i.e.,* one attached to a fluid parcel):

$$\frac{\partial \overline{c}}{\partial t} \;=\; \ldots \;-\; \boldsymbol{\nabla} \cdot \left(\overline{\mathbf{u}'c'} \right)\,. \tag{28}$$

The usual view is that rectification is associated with instabilities of the circulation, whereby the eddies cause mixing and dissipation in the dynamical balances for the mean quantities. Alternatively, eddy mixing can result from fluctuations forced, *e.g.,* by transient winds rather than by an instability. Mixing behaviors are embodied in the most common type of eddy parameterization, *eddy diffusion*,

$$
\begin{aligned}
\overline{\mathbf{u}'\mathbf{u}'} &= -\nu \boldsymbol{\nabla}\overline{\mathbf{u}} \\
\overline{\mathbf{u}'c'} &= -\kappa \boldsymbol{\nabla}\overline{c}\,.
\end{aligned}
\tag{29}
$$

Here ν and κ are positive eddy diffusivities chosen on the basis of some empirical knowledge of the eddy fluxes or expectation about the mean solution. Eq. (29) leads to diffusion operators in (27) and (28). It is also easy to see, by integration by parts ignoring boundary contributions (*i.e.,* boundary fluxes of momentum or material), that eddy diffusion is a sign-definite loss process for kinetic energy and tracer variance:

$$
\begin{aligned}
\frac{\partial}{\partial t} < \overline{\mathbf{u}}^2 > &= \ldots - < \kappa (\boldsymbol{\nabla}\overline{\mathbf{u}})^2 > \\
\frac{\partial}{\partial t} < \overline{c}^2 > &= \ldots - < \kappa (\boldsymbol{\nabla}\overline{c})^2 >\,,
\end{aligned}
\tag{30}
$$

where $< \cdot >$ denotes a spatial average. For $\nu, \kappa > 0$, the right-hand sides in (30) are non-positive.

An example of a situation where eddy diffusion is at least qualitatively valid is a broad (*i.e.,* $L \gg$) eastward jet with positive vertical shear, $\overline{\mathbf{u}}_z > 0$. By the thermal wind relation, it is associated with a negative meridional buoyancy or temperature gradient, $\overline{b}_y, \overline{T}_y < 0$, in the northern hemisphere where $f > 0$. If it is baroclinically unstable, buoyancy is transported towards the north by the eddy flux, $\overline{v'b'} > 0$. Therefore, the eddy diffusivity is positive,

$$\kappa \;=\; -\overline{v'b'}/\overline{b}_y \;>\; 0\,, \tag{31}$$

as expected, but the eddy viscosity in the core of the jet is negative,

$$\nu \; = \; -\overline{u'v'}/\overline{u}_y \; < \; 0 \,. \tag{32}$$

This behavior is relevant to both the mid-latitude westerly winds in the atmosphere and to the Antarctic Circumpolar Current (Chap. 4), although in both instances the fluctuations include important contributions from both transient currents and steady deviations from the zonal mean (*i.e.,* standing eddies).
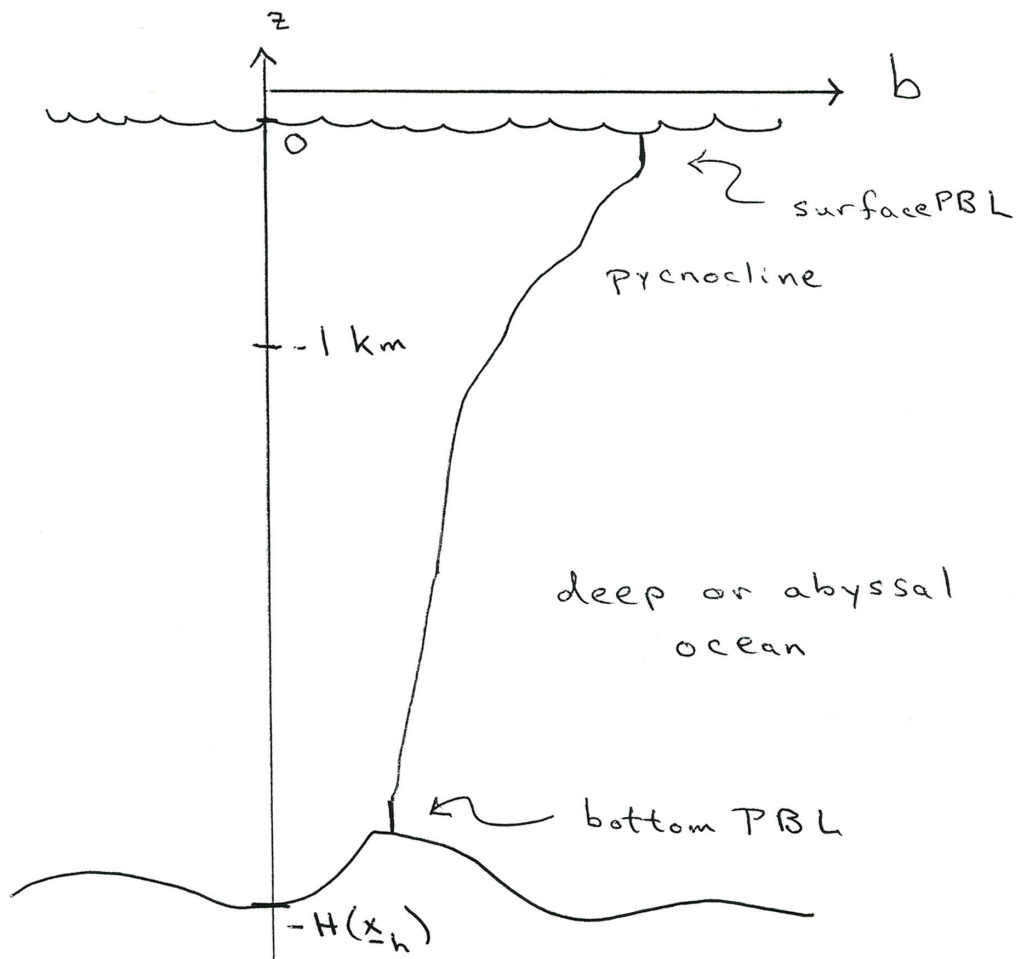
Figure 1: Schema of a typical vertical profile of buoyancy, $b = g[1 - \rho_\theta/\rho_o] = \int dz, N^2$, where g is the gravitational acceleration and ρ_θ is the potential density.
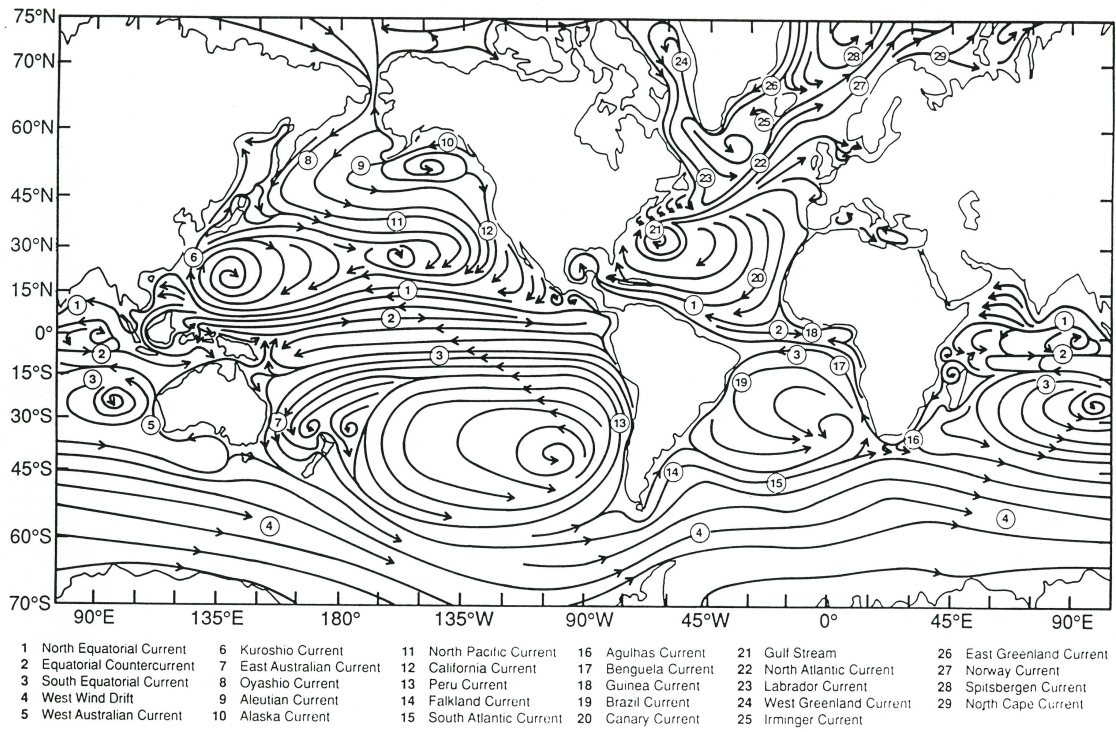
Major traditionally named ocean current systems of the world (Northern Hemisphere winter). (Adapted from Bowditch, 1966).

Figure 2: Schema of the surface circulation in the global ocean (Niiler, 1992).
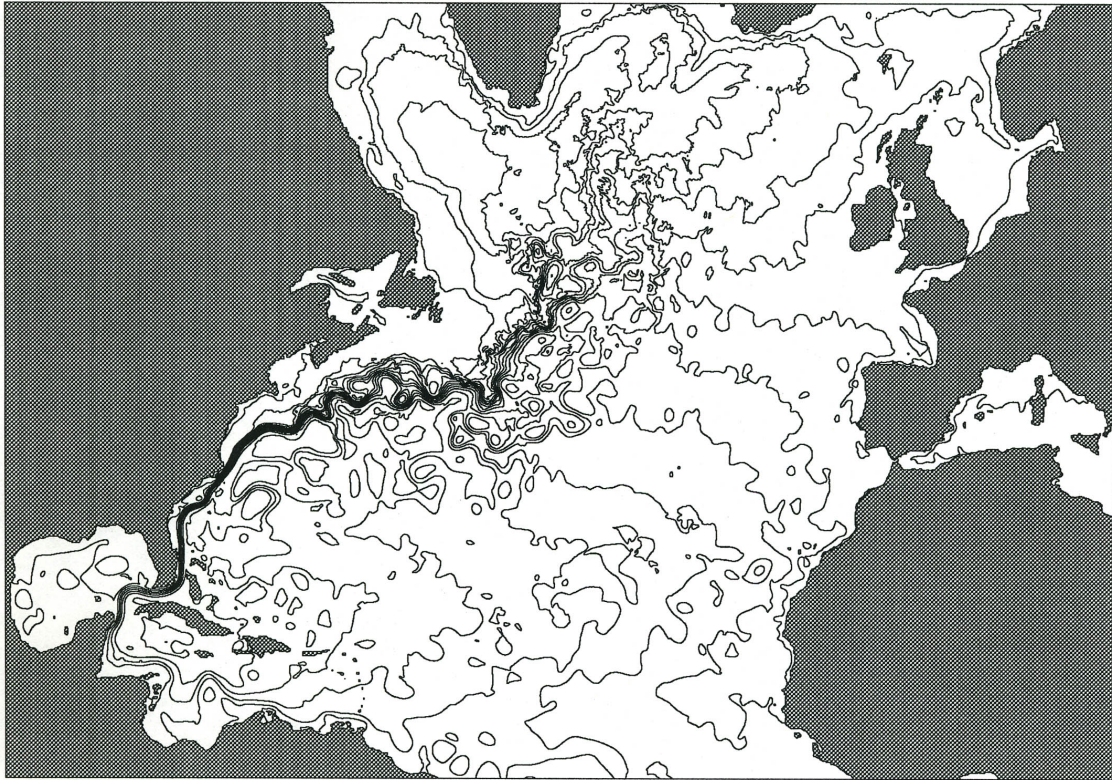
Figure 3: Instantaneous η in the North Atlantic as simulated in a high-resolution OGCM (McWilliams, 1996).
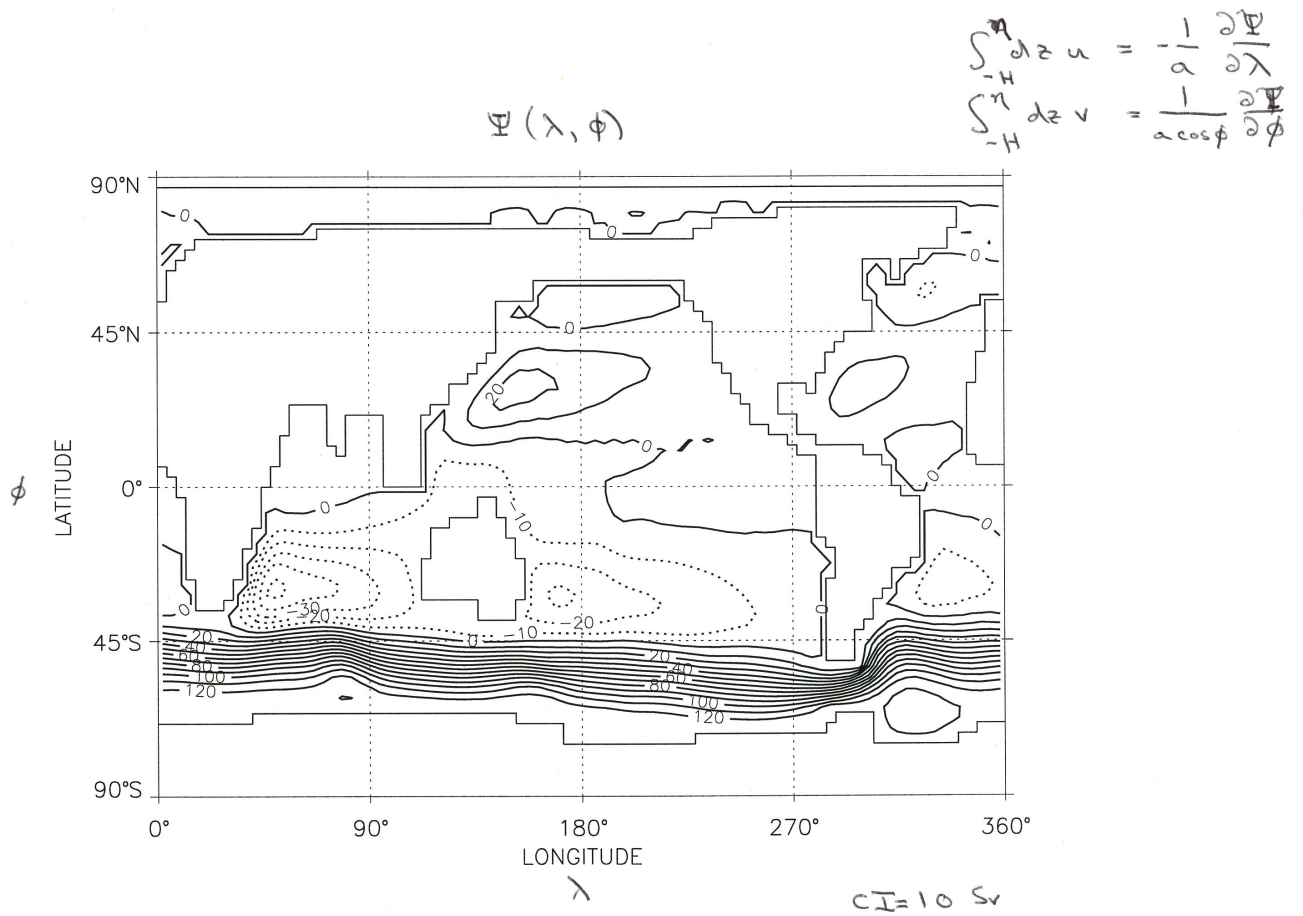
Figure 4: Steady-state, horizontal transport streamfunction in the global ocean as simulated in a coarse-resolution OGCM (McWilliams, 1996).

$$\Phi(\phi, z)$$
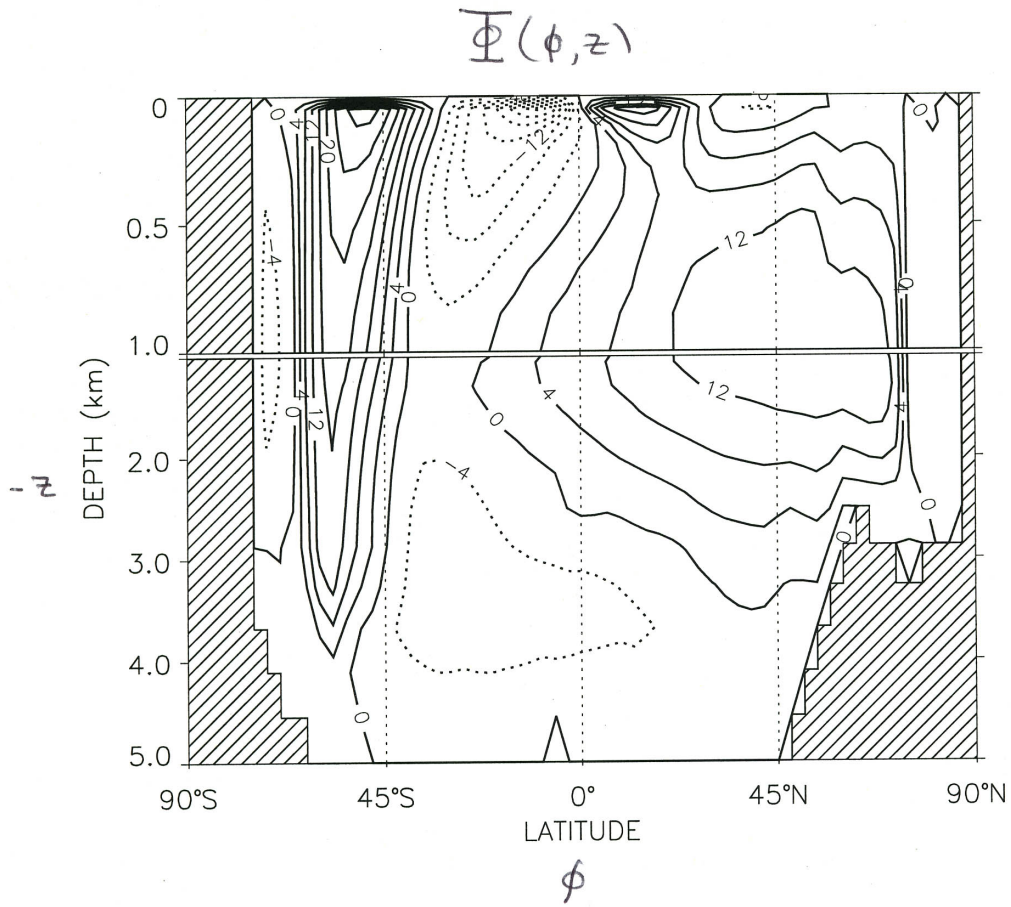
$$a\cos\phi \int d\lambda \, v = -\frac{\partial \Phi}{\partial z}$$

$$a\cos\phi \int d\lambda \, w = \frac{1}{a}\frac{\partial \Phi}{\partial \phi}$$

Figure 5: Steady-state, meridional overturning streamfunction in the global ocean as simulated in a a coarse-resolution OGCM (McWilliams, 1996).

26
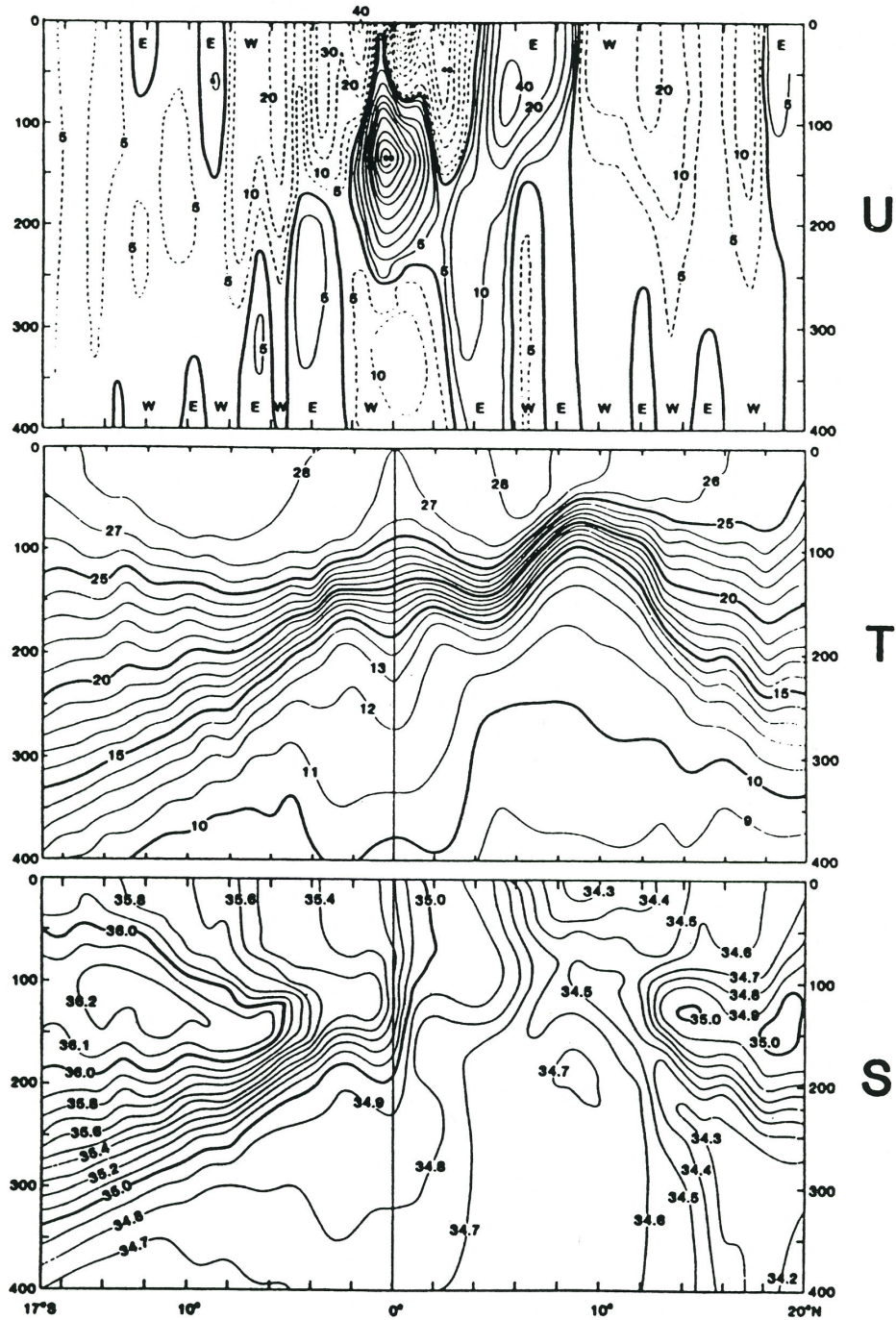
. Meridional cross sections of geostrophic zonal velocity, temperature and salinity at 155°W in the region between Hawaii and Tahiti. Note the bowing of the isotherms in the region of the EUC. The current is contained between the 15 and 25 °C isotherms. Note also the tongue of high-salinity water extending to the EUC, especially from the South Pacific. (From Wyrtki and Kolinsky 1984)

Figure 6: Meridional cross-sections of u (zonal velocity), T, and S in the central, equatorial Pacific from measurements (Wyrtki and Kilonsky, 1984).
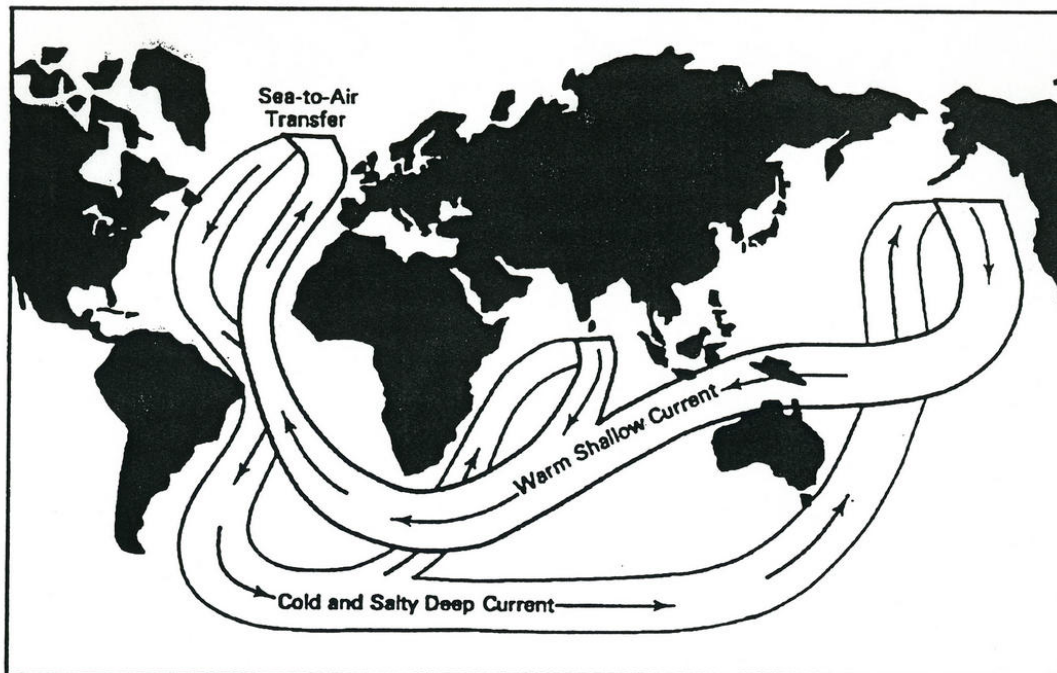
Figure 7: Schema of the global thermohaline circulation (Broecker, 1987).

Figure 8: Time- and zonal-mean T in the Atlantic from measurements (Levitus, 1982).
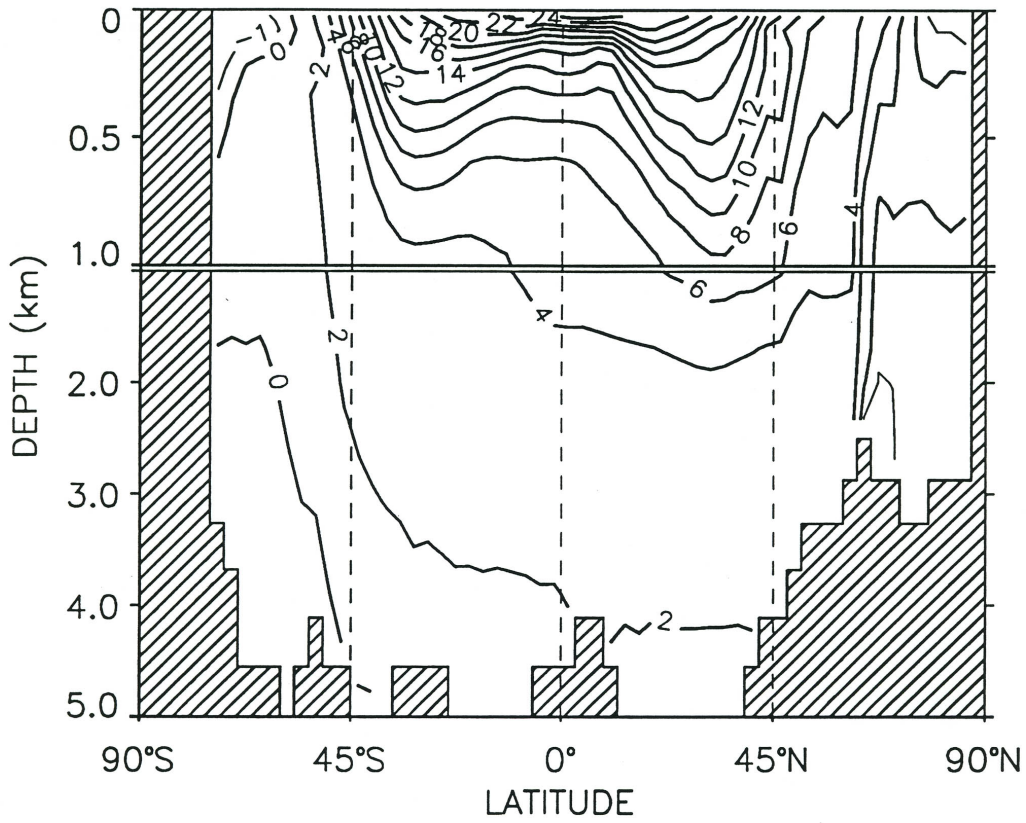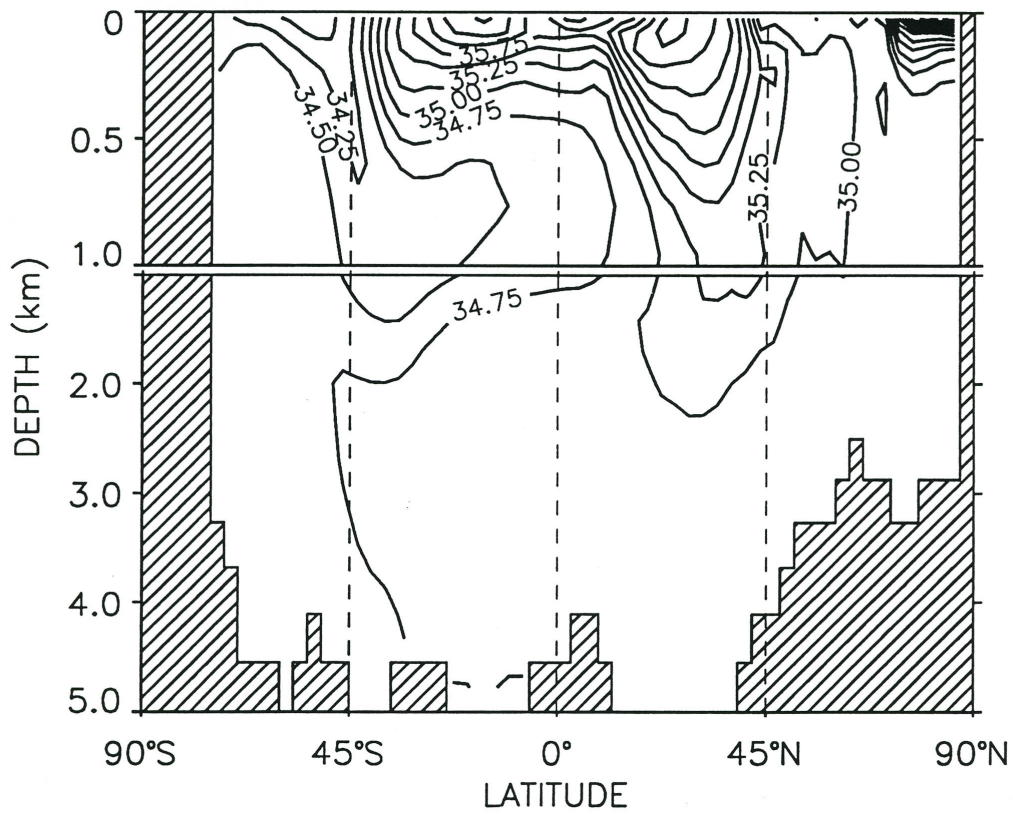
$$\overline{S}^{\lambda,t}(\phi,z) \text{ in the Atlantic}$$

$$(Levitus, 1982)$$

$$c.I. = 0.25 \text{ ppt}$$

Figure 9: Time- and zonal-mean T in the Atlantic from measurements (Levitus, 1982).
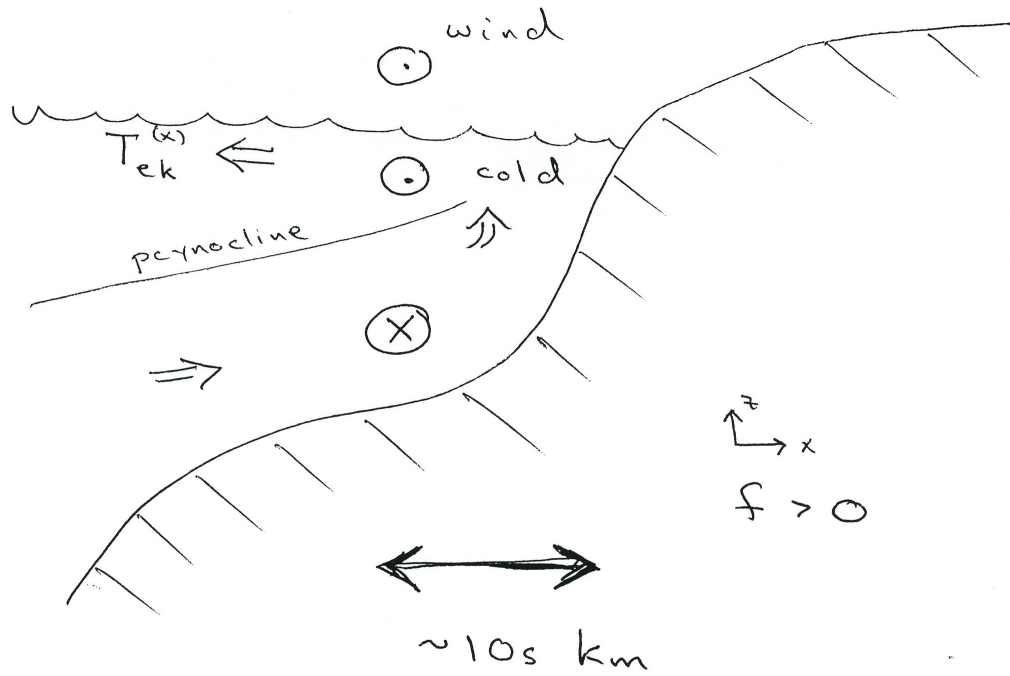
Figure 10: Schema of coastal upwelling circulation.
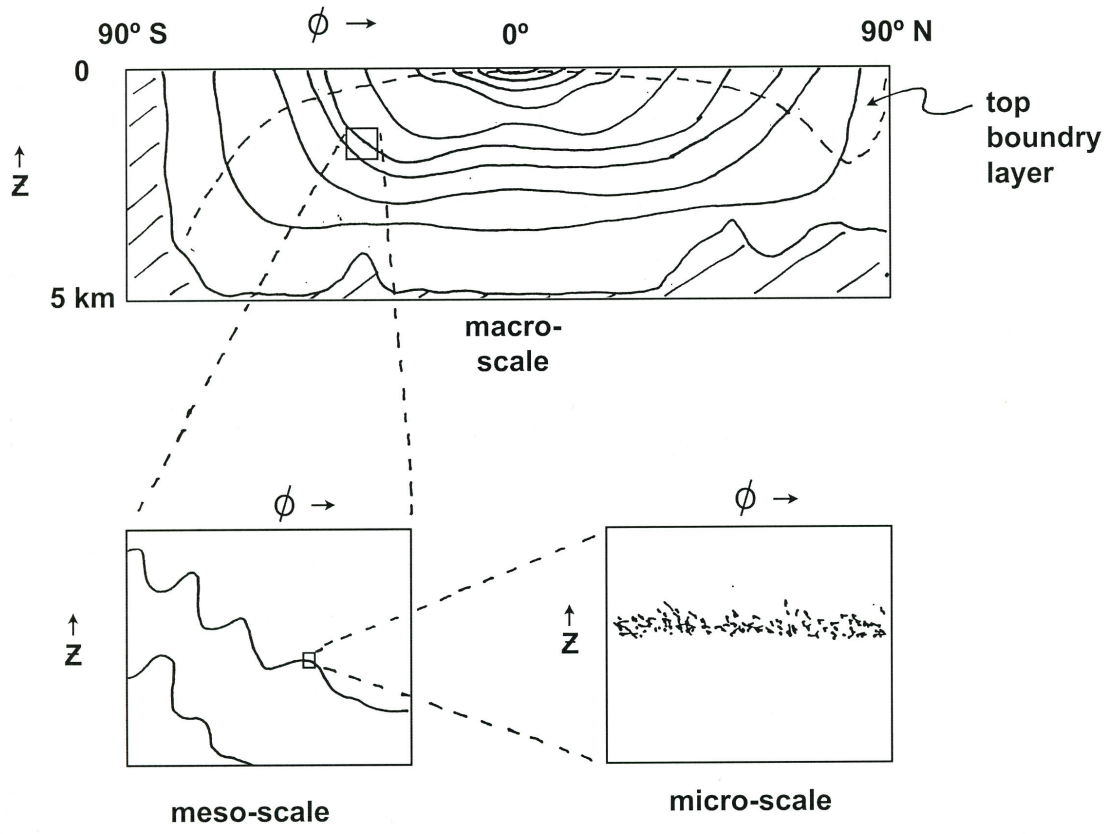
Figure 11: Schema of isopycnal surfaces in the meridional plane, viewed on three different spatial scales.
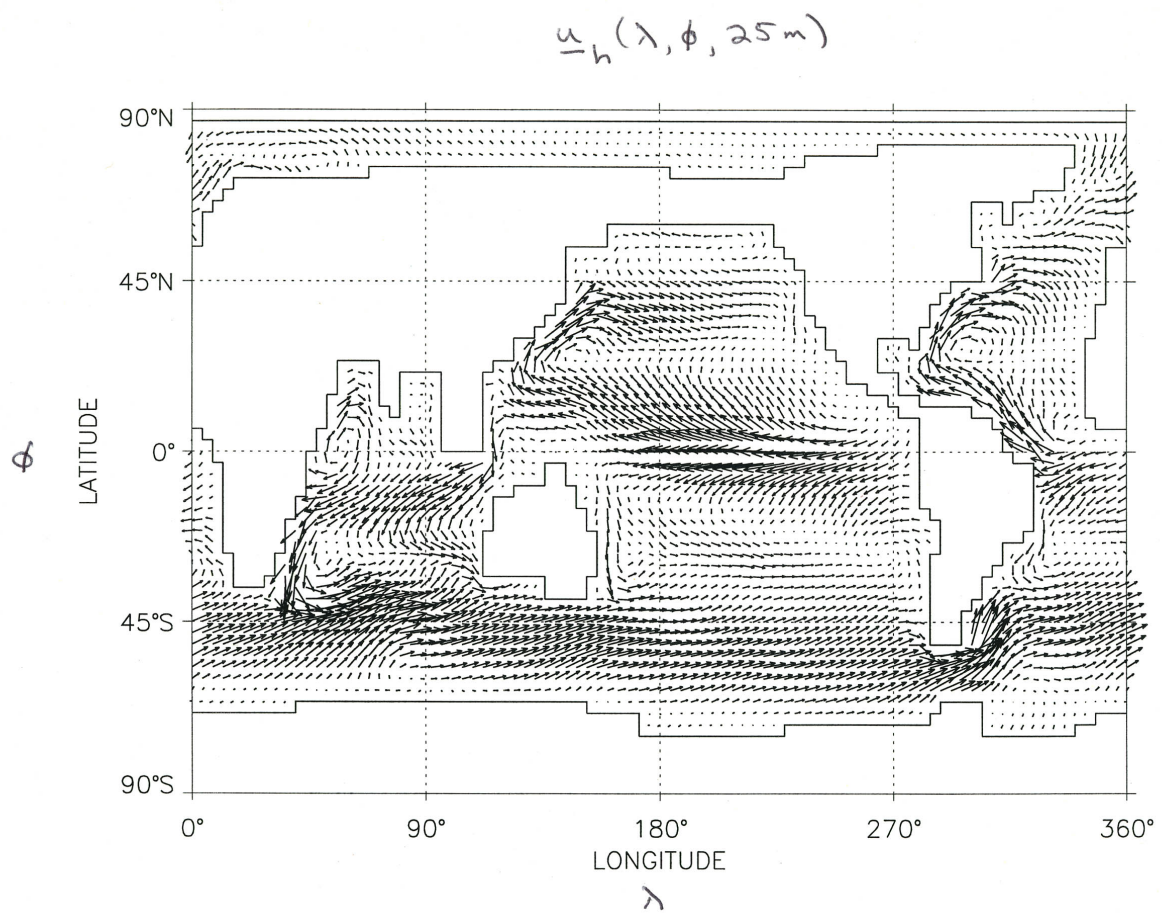
Figure 12: Steady-state $\mathbf{u}_h$ at 25 m depth in the global ocean as simulated in a a coarse-resolution OGCM (McWilliams, 1996).

(Rev. Geophys., 1998)

Non Critical $\rho - \Delta\rho$

η

V, H
specified ρ

b

Critical

dense   Critical
Point
Fr = 1   light

Controlled
Flow of
AABW
Through
Vema Gap

Figure 1. Sketch of an idealized flow of fluid along a channel with upstream velocity V and depth H, and the adjustment to a slowly increasing bottom b. The deflection downward of the interface is h.

Narrows
4000m
12°N
3500m
11°
>4500m
10°
3500m
40°W
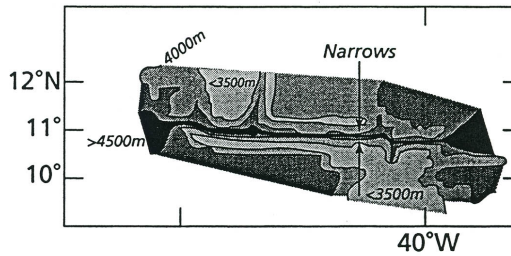
Figure 9a. Map showing the 3500-m, 4000-m, and 4500-m contours near the Vema Gap.

1.04595   1.04600   1.04605 ρ_4 $\left[\times 10^3 \, kg \, m^{-3} \right]$

3600

Depth (m)

4000

1000m

4600

$\Delta\rho = 5 \times 10^{-5}$

upstream

sill
depth

downstream

5000
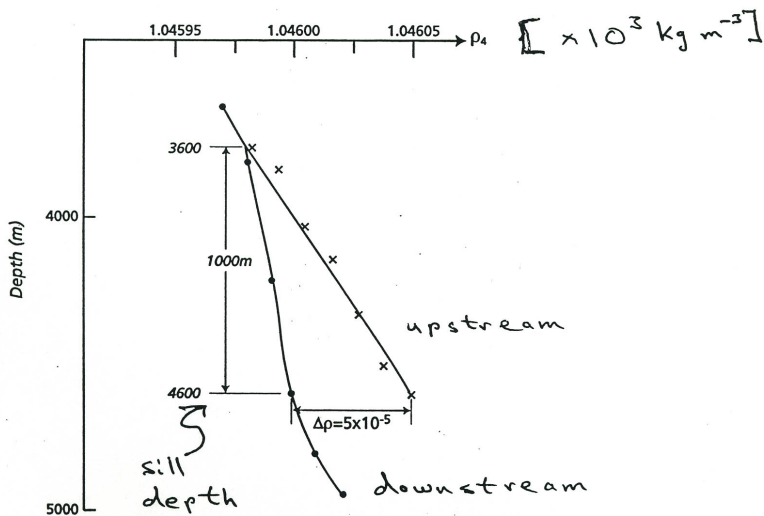
Figure 9b. Density (corrected to 4000 m) versus depth for selected stations upstream and downstream of Vema Gap.

. 13

Figure 13: Aspects of flow in a state of hydraulic control through the Vema Gap at the bottom of the central, tropical North Atlantic (Whitehead, 1998).
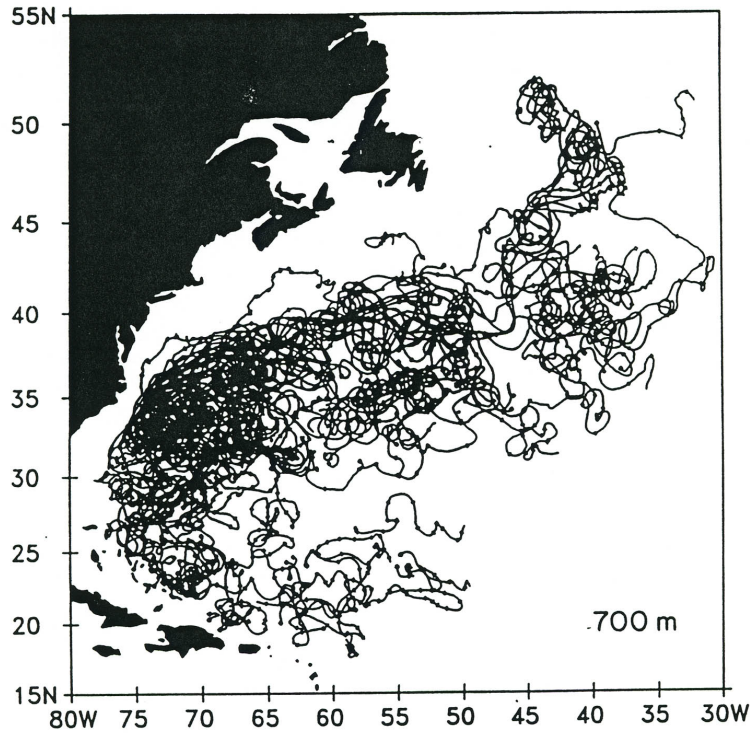
TRAJECTORIES OF
NEUTRALLY BUOYANT FLOATS

FIG.2. Trajectories for SOFAR floats at a nominal depth of 700m. Arrows along trajectories
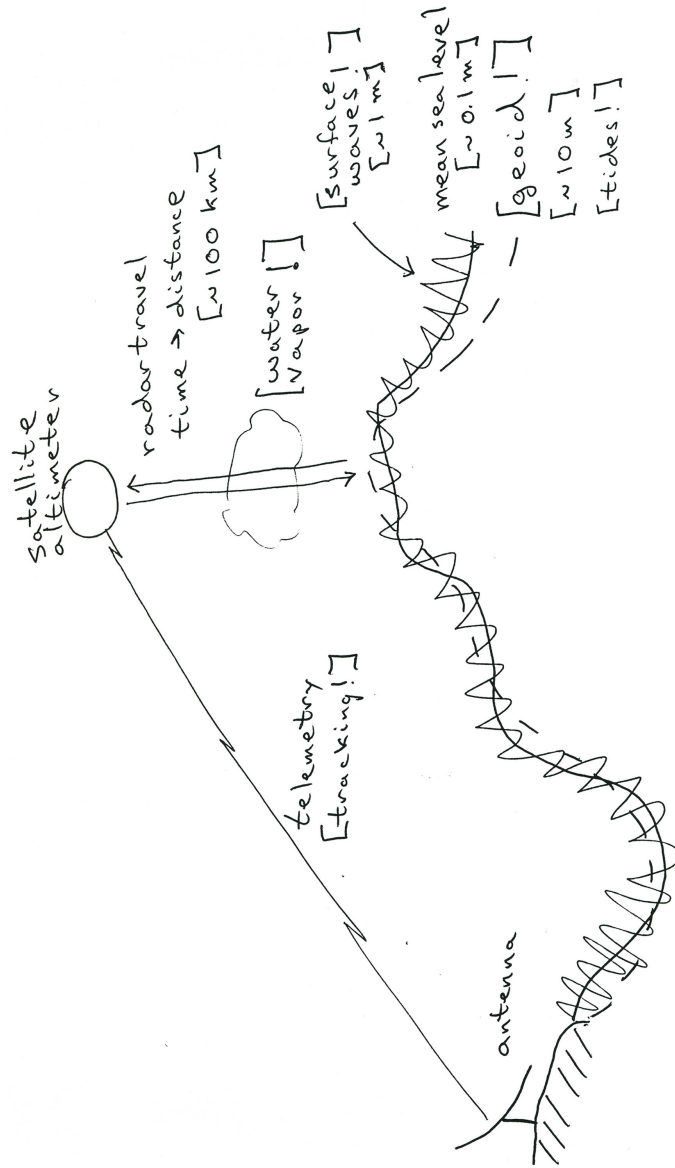occur on 30 day intervals.

(Owens, 1991)

MATERIAL DISPERSION :

$$\kappa_{\parallel} \equiv \frac{d}{dt} \frac{1}{2} \left\langle [\vec{x}(t) - \vec{x}(0)]^2 \right\rangle$$

$$\sim 10^3 \; m^2 s^{-1}$$

Figure 14: A "spaghetti" diagram of SOFAR float trajectories in the pycnocline of the northwestern
subtropical gyre in the North Atlantic (Owens, 1991).

35

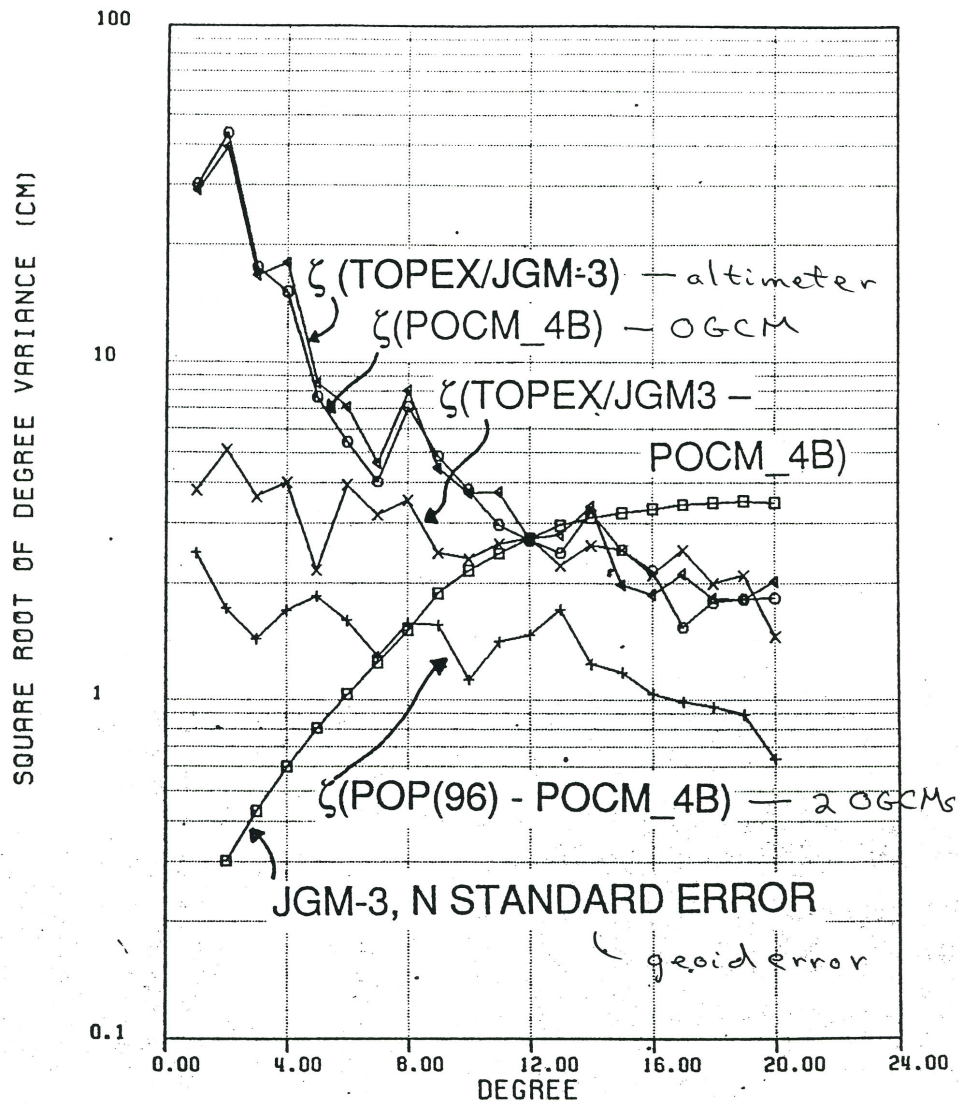Figure 15: Schema for satellite altimetry measurements.

Figure 3. Square root of degree variance of ζ from POCM_4B and TOPEX/JGM-3, JGM-3 undulation standard error, and the difference (POCM_4B − POP(96)), all in the ON system. Units are centimeters.

(Rapp et al., JGR 101, 22583-98, 1996)

Figure 16: Signal and error root-mean-square estimates for η, observed and modeled (Rapp et al., 1996). The abscissa is the order of a spherical harmonic.
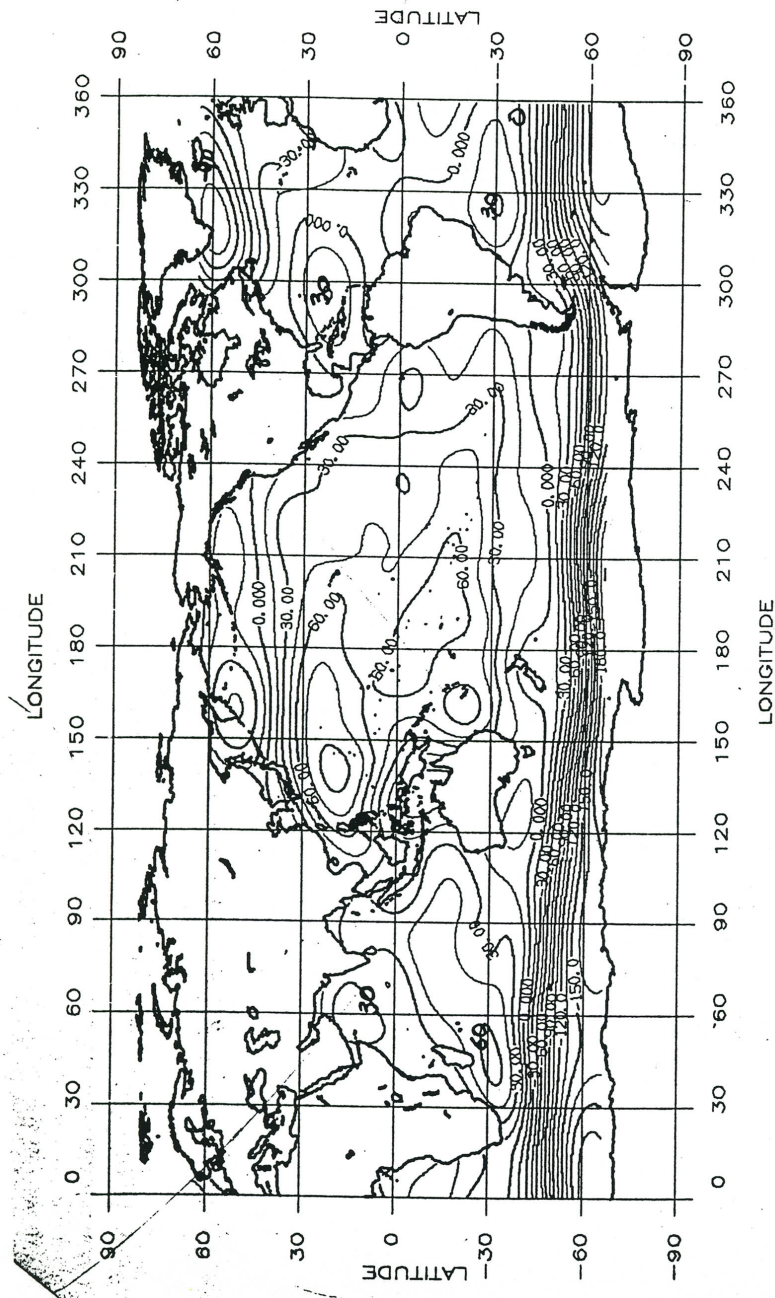
Figure 17: Dynamic topography, ϕ/g, averaged over two years of altimetric measurements (Rapp et al., 1996).
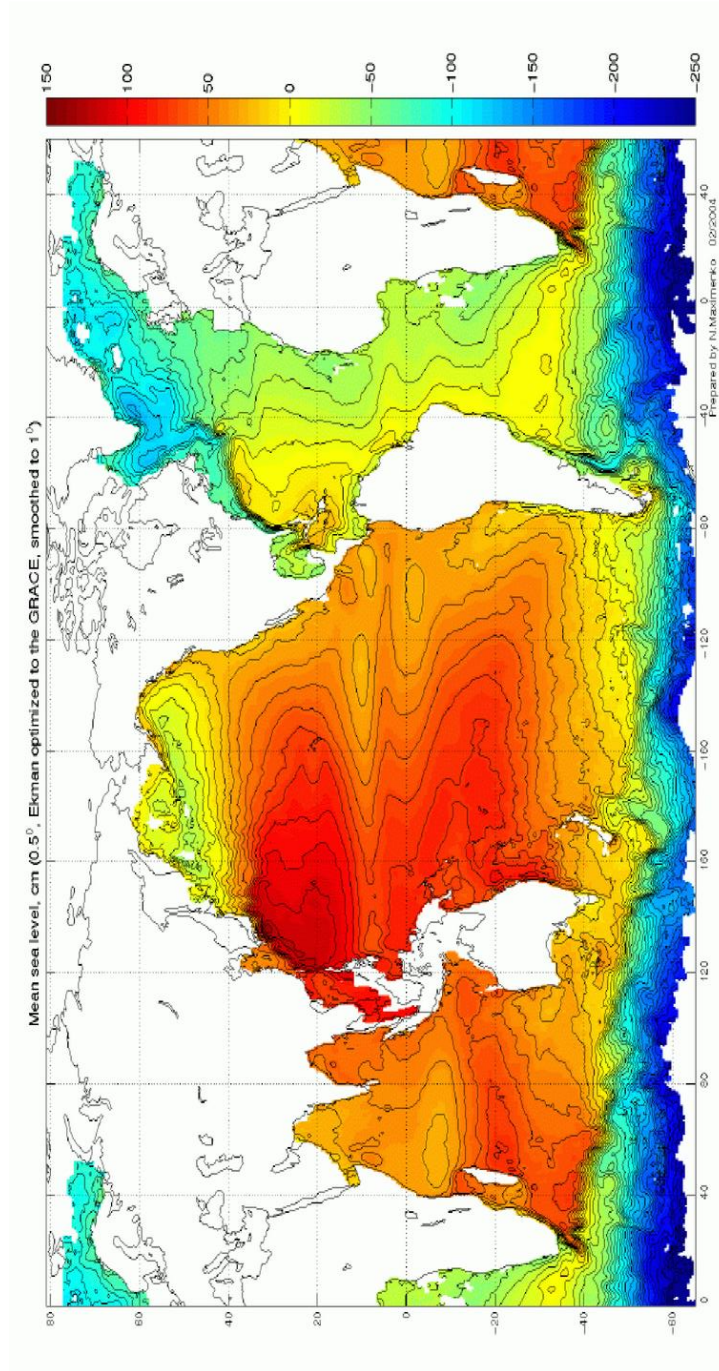
38

Figure 18: Observational estimate of time-mean sea level relative to a geopotential iso-surface, $\overline{\eta}$. The estimate is based on near-surface drifting buoy trajectories, satellite altimetric heights, and climatological winds. $g\overline{\eta}/f$ can be interpreted approximately as the surface geostrophic stream-function. Note the subtropical and subpolar wind gyres with sea-level extrema adjacent to the continental boundaries on western sides of the major basins and the large sea-level gradient across the ACC (Niiler et al., 2003).
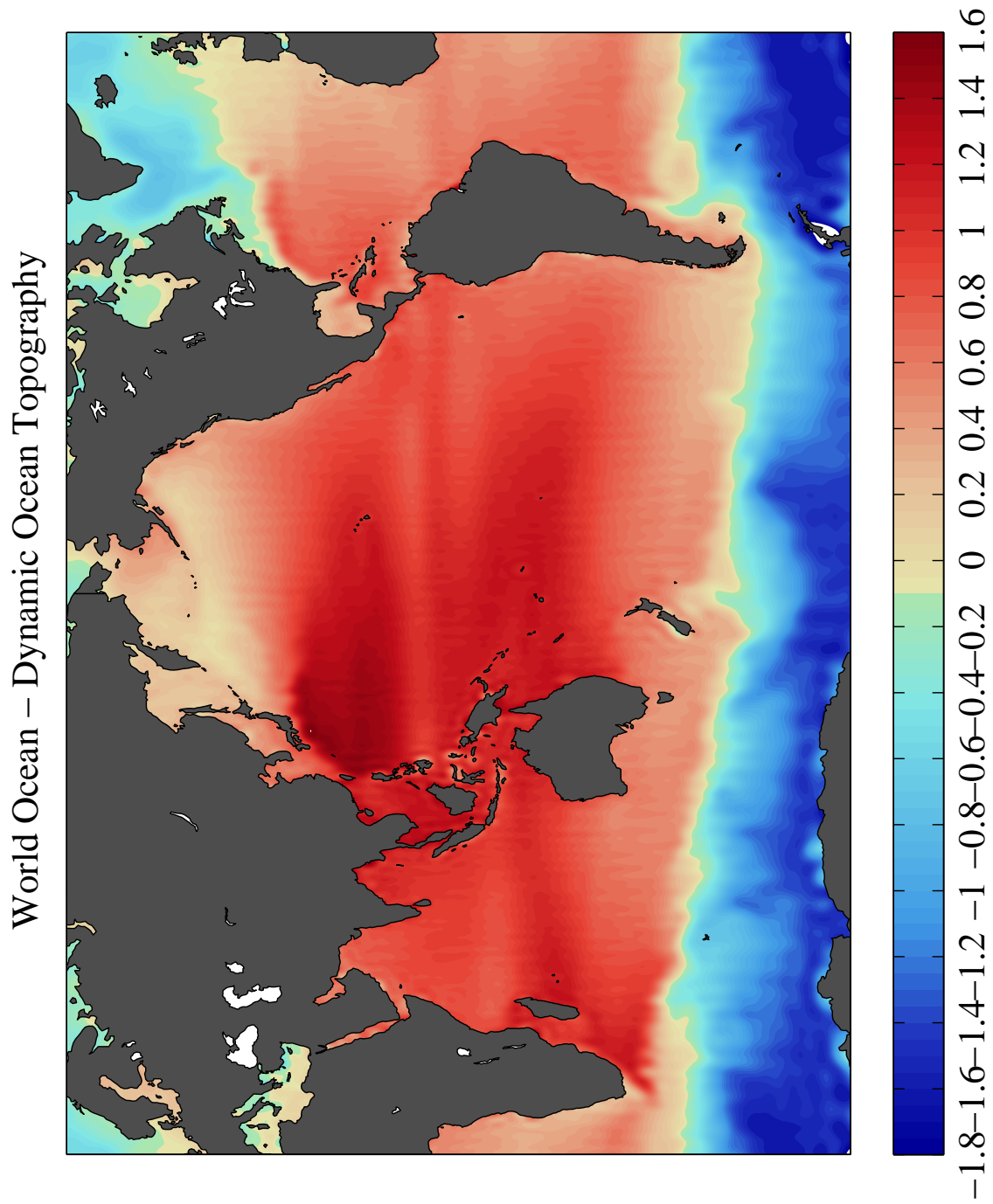
Figure 19: Observational estimate of time-mean sea level relative to a geopotential iso-surface, $\overline{\eta}$. This estimate is based on satellite alimetry and the improved geoid determined in the GRACE project (S. Jayne, personal communication).
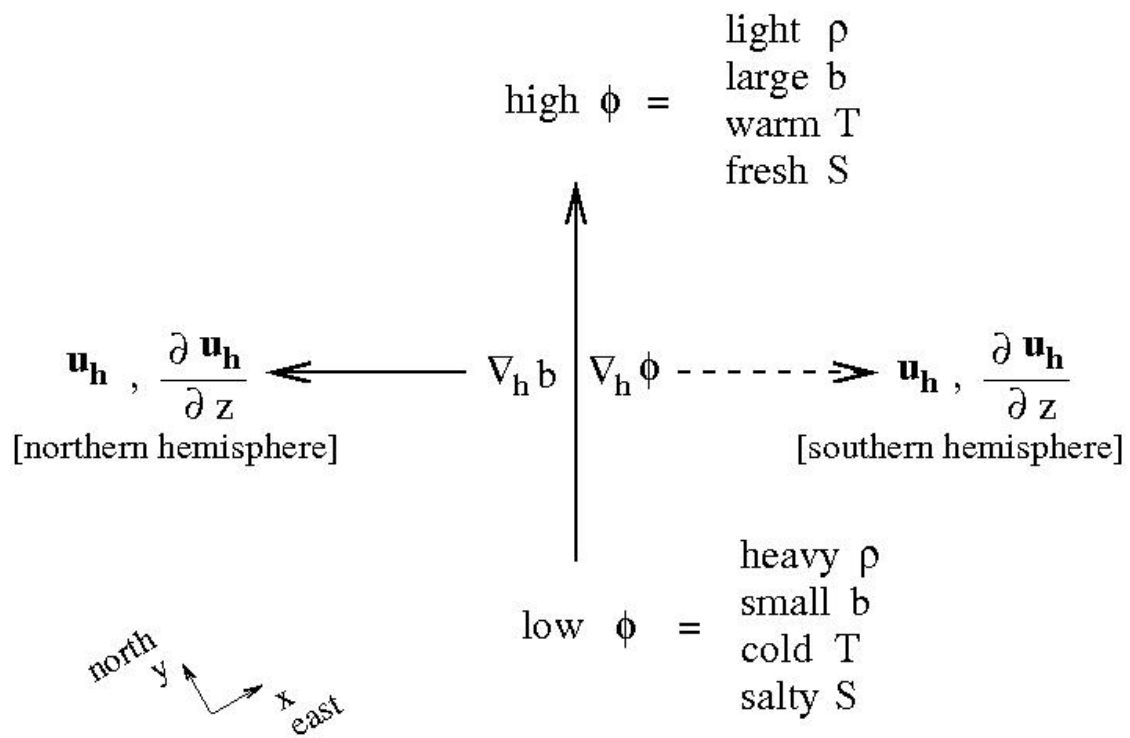
light ρ
large b
warm T
fresh S

high ϕ =

$\mathbf{u_h}$, $\dfrac{\partial \, \mathbf{u_h}}{\partial \, z}$ $\longleftarrow$ $\nabla_h b \, \big| \, \nabla_h \phi$ $- - - - \gg$ $\mathbf{u_h}$, $\dfrac{\partial \, \mathbf{u_h}}{\partial \, z}$

[northern hemisphere]   [southern hemisphere]

heavy ρ
small b
cold T
salty S

low ϕ =

north
y
x
east

Figure 20: Schema of geostrophic, hydrostatic relations among ρ, b, ϕ, T, S, and $\mathbf{u}_h$ or $\partial_z \mathbf{u}_h$.

References

Broecker, W., 1987: The biggest chill. *Nat. History*, **Oct.**, 71–82.

Bryan, K., 1969: A numerical method for the study of the circulation of the world ocean. *Comp. Phys.*, **4**, 347–376.

Chelton, D., J. Ries, B. Haines, L.-L. Fu, and P. Callahan, 2001: Satellite altimetry. *Satellite Altimetry and Earth Sciences*, L.-L. Fu and A. Casenave, eds., Academic Press, 1–131.

Jackett, D. and T. McDougall, 1995: Stabilization of hydrographic data. *Ocean Tech.*, **12**, 381–389.

Large, W., J. McWilliams, and S. Doney, 1994: Oceanic vertical mixing: A review and a model with a non-local K-profile boundary layer parameterization. *Rev. Geophys.*, **32**, 363–403.

Levitus, S., 1982: *Climatological Atlas of the World Ocean*. NOAA Prof. Paper 13, 173 pp.

Marchesiello, P., J. McWilliams, and A. Shchepetkin, 2001: Open boundary conditions for long-term integration of regional ocean models. *Ocean Modelling*, **3**, 1–20.

McDougall, T., 1987: Neutral surfaces. *J. Phys. Ocean.*, **17**, 1950–1964.

McWilliams, J., 1996: Modeling the oceanic general circulation. *Tellus*, **48A**, 179–192.

— 1998: Oceanic general circulation models. *Ocean Modeling and Parameterization*, E. C. . J. Verron, ed., Kluwer, 1–44.

Niiler, P., 1992: The ocean circulation. *Climate System Modeling*, K. Trenberth, ed., Cambridge University Press, 117–148.

Niiler, P., N. Maximenko, and J. McWilliams, 2003: Dynamically balanced absolute sea level of the global ocean derived from near-surface velocity observations. *Geophys. Res. Lett.*, **30**, 7–1 – 7–4.

Owens, W., 1991: A statistical description of the mean circulation and eddy variability in the northwestern atlantic using sofar floats. *Prog. Oceanog.*, **28**, 257–303.

Rapp, R., C. Zhang, and Y. Yi, 1996: Analysis of dynamic ocean topography using topex data and orthonormal functions. *J. Geophys. Res.*, **101**, 22583–22598.

Whitehead, J., 1998: Topographic control of oceanic flows in deep passages and straits. *Rev. Geophys.*, **36**, 423–440.

Wyrtki, K. and B. Kilonsky, 1984: Baroclinic theories of the wind-driven circulation. *General Circulation of the Ocean*, H. Abarbanel and W. Young, eds., Springer-Verlag, 134–201.